To the Graduate Council:

I am submitting herewith a thesis written by Janet E. Pawel entitled "Analysis of Adhesion Test Methods and the Evaluation of Their Use for Ion Beam Mixed Metal/Ceramic Systems." I have examined the final copy of this thesis for form and content and recommend that it be accepted in partial fulfillment of the requirements for the degree of Master of Science, with a major in Engineering Science.

Carl J. McHargue, Major Professor

We have read this thesis
and recommend its acceptance:

Jack F. Wasserman

Raymond A. Buchanan

Accepted for the Council:

Vice Provost
and Dean of The Graduate School

STATEMENT OF PERMISSION TO USE

In presenting this thesis in partial fulfillment of the requirements for a Master's degree at The University of Tennessee, Knoxville, I agree that the Library shall make it available to borrowers under rules of the Library. Brief quotations from this thesis are allowable without special permission, provided that accurate acknowledgment of the source is made.

Permission for extensive quotation from or reproduction of this thesis may be granted by my major professor, or in his absence, by the Head of Interlibrary Services when, in the opinion of either, the proposed use of the material is for scholarly purposes. Any copying or use of the material in this thesis for financial gain shall not be allowed without my written permission.

Signature Janet E. Powell

Date May 11, 1987

ANALYSIS OF ADHESION TEST METHODS AND THE EVALUATION OF THEIR USE FOR ION BEAM MIXED METAL/CERAMIC SYSTEMS

A Thesis

Presented for the

Master of Science

Degree

The University of Tennessee, Knoxville

Janet E. Pawel

June 1987

DEDICATION

This thesis is dedicated to my parents, Richard and Teresa Pawel, and to my brother, Steven, in appreciation of their tireless support, patience, and good humor.

ACKNOWLEDGEMENTS

The author would like to express her gratitude to her Major Professor, Dr. C. J. McHargue, for his support and guidance throughout the course of this research. Appreciation is also extended to Dr. J. F. Wasserman for his technical and professional guidance and to Dr. R. A. Buchanan for his many worthwhile suggestions.

Financial support provided under the Ceramic Technology for Advanced Heat Engines Program, Metals and Ceramics Division, Oak Ridge National Laboratory, administered by Dr. D. R. Johnson, is gratefully acknowledged.

The author is grateful to Mr. D. S. Easton and Mr. C.K.H. DuBose for technical assistance needed for thin film evaporation, to Dr. S. P. Withrow, Dr. T. P. Sjoreen, Dr. M. B. Lewis, and Mr. S. W. Cook for assistance with the ion beam mixing procedure, and to Dr. C. S. Yust for his advice on scratch testing. Technical assistance with scanning electron microscopy provided by Dr. T. F. Page, and additional microscopy and photography by the Metallography Group of the Metals and Ceramics Division, Mr. R. S. Crouse, Mr. T. J. Henson, Mr. B. C. Leslie, Mr. J. W. Nave, and Ms. C. L. Angel, are gratefully acknowledged.

Thanks are also extended to Mr. A. V. Blalock and Mr. J. S. Knisley for their assistance in operating and maintaining electronic equipment. The author would also like to acknowledge Mr. Blalock's contributions to equipment design and experimental procedure.

Special thanks are due to Mr. J. J. Campbell and Mr. D. S. Easton for their help with laboratory equipment and procedures.

The reliable and patient efforts of the departmental secretaries, Ms. Eunice Hinkle and Ms. Berdie Parsons, and particularly the author's ORNL secretary and typist, Ms. Lou Pyatt, is most gratefully acknowledged.

ABSTRACT

Several thin film adhesion tests have been examined to determine which provides the most reliable method for the measurement of the adhesion of thin metallic films to ceramic substrates. An attempt was made to use the testing techniques described to measure adhesion changes caused by ion beam mixing for a variety of metal/ceramic systems.

The testing techniques analyzed were the scratch test, the acoustic emission test, and the pull test. The major variables of the scratch test include film thickness, substrate hardness, and stylus radius but it is not known precisely what effects changes in these have on the measurement of adhesion. The scratch analyses methods discussed in the literature, each describing a load or stress on the system that is presumed to cause de-adhesion, do not always hold because none of the analyses account for both plastic and elastic deformation or incorporate many of the important parameters. The scratch test was much more likely to reveal a critical value for de-adhesion for relatively brittle films such as chromium than for ductile films such as nickel.

The acoustic emission test did not work for the scratch testing equipment used in this research. Whatever specimen emissions might have occurred were overshadowed by those of the drive motor, which could not be adequately isolated from the system.

An adaptation of the pull test, utilizing a thin gold layer under a portion of the test film, was developed because the adhesion of the test films was greater than the strength of the epoxy used in the standard test. Since this non-adherent layer served as a reproducible crack, the

analysis was analogous to that used in fracture toughness testing. Comparison of film adherence was based on the calculation of the stress intensity factor necessary to cause film de-adhesion. The results of this modified pull test were very promising and involved fewer parameters than the scratch test.

Scratch test data for most of the systems exhibiting critical values for de-adhesion revealed that ion beam mixing significantly improved the adhesion of the films to their substrates. Ion beam mixed films also withstood a greater applied tensile stress and a greater stress intensity factor without de-adhesion than unmixed films with similar flaws.

TABLE OF CONTENTS

CHAPTER		PAGE
I.	INTRODUCTION	1
II.	LITERATURE REVIEW	3
	Testing Methods	3
	The Scratch Test	3
	Introduction	3
	Complexities of the scratch test	5
	Variations in film thickness	7
	Variations in substrate hardness, stylus hardness, and stylus radius	9
	Analyses of the scratch test	9
	The Acoustic Emission Test	22
	Introduction and analysis	22
	Use in scratch testing	26
	Use in other tests	27
	The Pull Test	27
	Introduction	27
	Variations in cement thickness and bond strength	28
	Fracture energy analysis	29
	Ion Beam Mixing	30
	Introduction	30
	Effect on Adhesion	31

CHAPTER PAGE

III. EXPERIMENTAL PROCEDURE 32
Substrate Materials 32
Substrate Cleaning Procedure 32
Film Deposition 33
Specimen Characterization 34
Scratch Test 36
Acoustic Emission Test 38
Pull Test 39
Ion Beam Mixing 39
IV. RESULTS AND DISCUSSIONS 41
The Scratch Test 41
Systems Analyzed 42
Aluminum films on glass 42
Nickel and chromium films on sapphire 42
Zirconium films on sapphire 42
Scratch Characteristics 43
System vibrations and noise 43
Characteristics of the scratch path 43
Deformation modes 56
Analyses 63
Variations in styli and film thickness 63
Analysis based on normal load criterion 64
Analysis assuming full plasticity 64
Analysis assuming elastic conditions 69

CHAPTER PAGE

IV. (Continued)

The Pull Test 74

Effects of Ion Beam Mixing 81

Adhesion to Sapphire Substrates 81

Scratch adhesion 81

Tensile adhesion 87

Adhesion to Silicon Carbide and Silicon Nitride Substrates 88

Aluminum film on silicon nitride 91

Aluminum film on silicon carbide 92

Zirconium film on silicon carbide 93

Zirconium film on silicon nitride 103

V. CONCLUSIONS 110

The Scratch Test 110

The Pull Test 113

Effects of Ion Beam Mixing 113

LIST OF REFERENCES 116

VITA 123

LIST OF TABLES

TABLE		PAGE
1.	Shear Stresses Calculated Using the Plastic Model Analysis for Scratches on Zirconium/Sapphire	66
2.	Shear Stresses Calculated Using the Plastic Model Analysis for Scratches on Chromium/Sapphire	67
3.	Shear Stresses Calculated Using the Plastic Model Analysis for Scratches on Nickel/Sapphire	68
4.	Shear Stresses Calculated Using the Plastic Model Analysis for Scratches on Aluminum/Glass	70
5.	Shear Stresses Calculated Using the Elastic Model Analysis for Scratches on Zirconium/Sapphire Comparing the Results Obtained for Different Values of Young's Modulus, E	73
6.	Radial and Shear Stresses Calculated Using the Elastic Model Analysis for Scratches on Chromium/Sapphire	75
7.	Radial and Shear Stresses Calculated Using the Elastic Model Analysis for Scratches on Nickel/Sapphire	76
8.	Pull Test Results for Specimens with Gold Release Layer	80
9.	Stresses Recalculated Assuming Reduced Area Under the Pin by Omitting Area Over the Gold Release Layer	82
10.	Comparison of Critical Shear Stresses Calculated Using the Plastic Model Analysis for Scratches on Chromium/Sapphire	85
11.	Comparison of Critical Shear Stresses Calculated Using the Elastic Model Analysis for Scratches on Chromium/Sapphire	86
12.	Pull Test Results for Ion Beam Mixed Specimens	89
13.	Pull Test Strength of Aluminum Film on Silicon Carbide Substrate	94
14.	Pull Test Strength of Zirconium Film on Silicon Carbide Substrate	98
15.	Pull Test Strength of 515 nm Zirconium Film on Silicon Nitride Substrate	105

TABLE PAGE

16. Pull Test Strength of 530 nm Zirconium Film on Silicon Nitride Substrate 109

17. Analysis Methods Useful in the Determination of Critical Values for Film De-adhesion for the Systems Investigated . . 112

LIST OF FIGURES

FIGURE		PAGE
1.	Forces at the lip of the stylus indentation as assumed by Benjamin and Weaver	11
2.	Schematic view of the stylus on the surface	13
3.	Points of maximum yield parameter below the stylus for various coefficients of friction	14
4.	Stretching of the film during indentation	16
5.	Typical scratch profile made with a 0.2-mm radius stylus tip	19
6.	Schematic representation of the crack formed ahead of the stylus moving from left to right	20
7.	Height profile across the end of the channel showing the crack formed ahead of the stylus	21
8.	Model of failure by the scratch test	23
9.	Electron beam power as a function of time for the deposition of the zirconium films	35
10.	The scratch tester	37
11.	Stylus skipping caused by system vibrations	44
12.	Scratch made on aluminum/glass system under a normal load of 2.0 g	45
13.	Typical scratch profiles	46
14.	Scratch made on zirconium/sapphire specimen under a normal load of 30 g	48
15.	Scratch made on zirconium/sapphire specimen under a normal load of 40 g	49
16.	Scratch made on nickel/sapphire specimen under a normal load of 150 g	50
17.	Scratches made on aluminum/glass specimen under a normal load of 0.45 g	51

FIGURE PAGE

18. Scratches made on aluminum/glass specimen under a normal load of 1.0 g 52

19. Full length view of scratches in Figures 17 and 18 before ultrasonic cleaning 53

20. Thinning of zirconium film under normal stylus loads of (a) 10 g and (b) 200 g 54

21. Effect of surface flaw on scratching of zirconium/sapphire system 55

22. Transverse profile of a scratch showing ductile extrusion of nickel film on a sapphire substrate 57

23. Transverse profile of a scratch showing absence of ductile extrusion of a chromium film on a sapphire substrate 58

24. Scanning electron micrograph of a 250-g normal load scratch on a chromium/sapphire specimen 59

25. Two regions of compressive failure caused by a 450-g normal load scratch on a zirconium/sapphire specimen 60

26. Tensile failure behind the moving stylus caused by a 400-g normal load on a zirconium/sapphire specimen 61

27. Theoretical line of constant maximum tensile stress acting in the plane of the surface for a friction coefficient of 0.25 62

28. Theoretical and experimental values of the radius of the circle of contact for scratches on aluminum/glass specimens 71

29. Original 30 nm zirconium film on silicon carbide 90

30. Dark spots of film removed with the test pins 97

31. De-adhesion of zirconium film from silicon carbide specimen surface in unmixed regions 99

32. De-adhesion of Figure 31 at higher magnification 100

FIGURE PAGE

33. Zirconium on silicon carbide specimen surface, ion beam mixed to a dose of 0.5×10^{16} ions/cm^2 101

34. Zirconium on silicon carbide specimen surface, ion beam mixed to a dose of 2.0×10^{16} ions/cm^2 102

35. Zirconium (515 nm) on silicon nitride specimen surface in unmixed region 106

36. Zirconium (515 nm) on silicon nitride specimen surface in mixed region 107

CHAPTER I

INTRODUCTION

Thin films can be used to make a monolithic material suitable for special requirements in a variety of applications. Such films can be used to provide resistance to wear, corrosion, abrasion, erosion, galling, tarnish, radiation damage, or high temperature oxidation as well as to reduce electrical resistance and friction. They also can provide lubrication, prevent sticking, and provide special magnetic or dielectric properties (1). The use of thin metallic films on ceramic substrates represents an important area. Specifically, the films in this research are used as electrical contacts for semiconductors and as intermediate layers to enhance the adherence of thermal barrier coatings. The effectiveness, durability, longevity, and strength of a film all depend intimately on the degree of adhesion between the film and its substrate. One of the goals of this research is the determination of a reliable method for the measurement of the adhesion of thin metallic films to ceramic substrates. Measurement of adhesion of ductile metallic films on brittle ceramic substrates poses a problem, however, because the "cotton-bud" test (removal of a film by rubbing with a cotton swab) and the "3M" test (removal of a film by plastic tape) are highly qualitative, whereas the widely used quantitative tests have found the most success with brittle films on ductile substrates. Also, adhesion tests often yield no clear separation between the film and its substrate and different testing methods give different values of adhesion.

One method of improving the interfacial bonding between a film and its substrate is by a form of ion implantation called ion beam mixing in which the film is bombarded with heavy ions of sufficient energy to penetrate the film and enter the interfacial region. A second goal of this research is to investigate the adhesion change as a function of ion beam mixing for several systems.

The testing methods analyzed and discussed in this paper are the scratch test, the acoustic emission test, and the pull test. The various aspects and parameters of each test must be recognized and understood before any significance can be given to the data. A brief introduction to ion beam mixing and its effects on thin film adhesion is included in the literature review and an attempt is made to use the testing techniques described to measure adhesion changes caused by ion beam mixing for a variety of systems.

CHAPTER II

LITERATURE REVIEW

Testing Methods

The Scratch Test

Introduction. The scratch test was developed by Benjamin and Weaver (2) from a technique originally described, but not analyzed, by O. S. Heavens in 1950. In this method, a smoothly rounded stylus point is drawn across the film surface. The vertical load on the stylus is increased until the film is stripped from the substrate. The critical load is defined as that load on the stylus at which the coating is stripped cleanly from the substrate.

By varying substrate materials for the same film material, Benjamin and Weaver found that the critical load did depend on the nature of the substrate but saw no direct relation between the critical load and the substrate hardness or elasticity. The critical load also varied with film material (on the same substrate) but did not correlate with a specific film property such as hardness. Furthermore, for films exceeding a certain thickness, the critical load became constant; a continuous variation with thickness would be expected if the load depended on some mechanical property of the film. From these results, they concluded that the critical load is determined by the interfacial properties of the system.

Analysis of the horizontal forces led Benjamin and Weaver to the following proposal. When a rounded point is drawn across a coated

surface, and the adhesion of the point to the coating is good, shearing must occur at the weakest point, either at the coating/substrate interface or within the substrate. Assuming that the cohesive forces within the substrate are greater than the adhesive forces of the interface, the shearing should occur at the interface and thus the force should be less than the shearing found when the stylus is passed over the uncoated substrate material and only cohesive shearing is possible. When the adhesion of the point to the coating is poor, the stylus slides over the film for increasing normal loads until the deformation of the substrate is sufficient to loosen the film. Since the substrate is plastically deformed, the metal film is also deformed to the indentation shape. This causes the film to stretch and a shearing force to develop between the film and the substrate. This shearing force increases with increasing load until the adhesive bonds between the substrate and film are broken at the lip of the indentation, where the shearing forces are maximum. Once the de-adhesion occurs at the lip of the indent, the shearing extends over the whole indentation. The stylus continues to deform the substrate as it travels, shearing adhesive bonds over the advancing profile and pushing the sheared material aside. The authors found, experimentally, that the former is not the case but that the latter analysis involving the deformation of the substrate is in close agreement with the experimental evidence, especially since plastic deformation of the substrate was observed in every case.

Benjamin and Weaver developed an equation relating the shearing force per unit area to the stylus load, stylus radius, and substrate

hardness. Comparison of this equation using experimental data with calculations of the force required to overcome van der Waals forces at the interface show that the former gives numbers of the same order of magnitude as the latter. Further experiments revealed that the critical load increased with stylus radius but that the shearing force, as calculated from their equation, remained reasonably constant.

Complexities of the scratch test. Since Benjamin and Weaver's work in 1960, many other researchers have investigated the scratch test and have concluded that it is much more complex than the original analysis implied (3-12). Even Benjamin and Weaver (2) admitted that their theory was based on an idealized indentation shape and that they had neglected elastic deformation.

Butler, Stoddart, and Stuart (3) found that detached film could be pressed back into the path by the stylus or that a film could be thinned to transparency without detachment, and thus the critical load could not be determined on the basis of a clear stylus track. They also indicated that a much larger number of parameters of the film, such as yield stress, surface condition, density, and grain size, also are factors in apparent adhesion differences. In addition, they pointed out the sequence of yield in the film, interfacial region and substrate may be controlled by many factors. These remarks have been verified by others (8,9).

In 1975, Charles Weaver (5) concluded, using scanning electron micrographs of the scratch path which showed hillocks ahead and to the

side of the stylus, that the original theory of detachment by shearing could not be valid.

Laeng and Steinmann (6) pointed out the importance of the failure mode, not only that it affects the value of the critical load, but that some modes do not show a straightforward track clearing but involve local flaking. They advised careful examination of the scratches. Je, Gyarmati, and Naoumidis (11) also reported that the mode of coating failure varies with the substrate material, film material, film thickness, and the method by which the film is produced.

Laugier (7) showed friction to play a critical and complex role in the film stripping process. This is discussed in more detail in a later section.

Partial elastic recovery of the substrate was noted by Perry (8), and Perry, Laeng, and Hintermann (9) pointed out that substrate surface roughness may be a factor. Perry (13) later reported a dependence on shear moduli and concluded that the relationship between the critical load and the actual adhesion strength is not yet understood.

In 1986, Valli, Makela, and Matthews (12) noted that adhesion may seem to be improved in an inferior film because a film that is porous can more readily accommodate deformations. They also reported a dependence of the data on indenter material, film surface finish and geometry, coating surface condition and geometry, and air humidity during testing.

In spite of all of the ambiguities and complexities of the scratch test, many researchers consider it to be the best of the many adhesion

tests (2,10,12) and realize that it has great value as a comparative test, particularly for films on the same substrate (6,14) or the same film/substrate systems (3,4,12,13,15,16). Weaver and Parkinson (17) used the scratch test to study the diffusion of gold and aluminum layers on a substrate and obtained such consistent results that this experiment is considered convincing evidence that the critical load is determined primarily by the adhesion between film and substrate (5). Mehrotra and Quinto (18) pointed out that, for their work, the critical load values from duplicate scratches were almost identical.

However, critical loads determined from the scratch test are often reported as being within some scatterband or using histograms, as they can vary significantly for identical systems (10,13,19). Weaver (5) noted that low measurements of adhesion can be easily explained as weak spots and suggested that the highest values are closest to the true adhesion. Perry (13) on the other hand, utilized the criterion that the onset of loss is decisive because this is soon followed by general failure in practice. He also reported that the criterion of taking the first local loss of film as the critical load or the regular loss along the scratch path makes little difference within the scatterband.

Variations in film thickness. There has been some controversy over the effect of film thickness on the critical load. Benjamin and Weaver (2) reported that the critical load became constant for films exceeding a certain thickness. The initial sloping part of the load versus film thickness curve, Benjamin and Weaver stated, is not due to a

defect of the method but rather due to film structure, which may not be continuous at small thicknesses.

Chopra (20), after reviewing the work of Benjamin and Weaver, noted that their conclusion is only valid for peeling of the film under the critical load. Since in practice the stylus scratches the film, the critical load is determined by the mechanical properties of the film as well as adhesion. Chopra's experimental results do indeed show a strong dependence on film thickness for film thicknesses greater than about 200 nm. From his data, Chopra concluded that for film thicknesses less than 200 nm the critical load is a reasonable measure of adhesion.

The work of Butler, Stoddart, and Stuart (3) also showed that a greater load was required to thin a thick soft film to transparency than for a thin soft film. In addition, different detachment modes were observed for the thick and very thin films. The authors explained their results using the analysis of Hamilton and Goodman (21) for a sphere impressed on a semi-infinite flat surface. For this case, plastic deformation can first occur, not at the surface, but within the body, and at a distance on the order of the film thicknesses studied here. Thus, a very thick film may contain the initial yield point but plastic deformation may occur first in the substrate under a thin film.

Perry (13,22), like Chopra, found that the critical load increased with coating thickness. In his analysis, the scratch test involves the inducement of a shear stress at the interface as a result of deformation of the system, therefore a thicker layer may require a greater surface load to attain the same shear stress at the interface. Je, Gyarmati,

and Naoumidis (11) concurred with Perry's results and conclusion. Perry and Pulker (23) noted the same phenomenon and also that the behavior of large film thicknesses was less reproducible due to the effect of mechanical stress in the film on the adhesion. Laeng and Steinmann (6) and Hammer, et. al. (10), also reported the increase of the critical load with increasing film thickness.

In contrast, Kikuchi, Baba, and Kinbara (19) found that for the systems studied in their work, the mean value of adhesion was almost independent of film thickness.

Variations in substrate hardness, stylus hardness, and stylus radius. The critical load has been found to increase with substrate hardness (10,13), and stylus hardness (19), although Hamersky (24) found it to be indirectly dependent on stylus hardness. Also, Hamersky obtained reproducible results only while using a stylus radius larger than 0.2 mm; Laeng and Steinmann (6) verified Hamersky's conclusion of critical load dependence on stylus radius.

Analyses of the scratch test. Benjamin and Weaver (2) found the shearing force per unit area, F, based primarily on the classical equations of Hertz describing the deformation of a flat surface under a hard sphere. For purely elastic deformation, the radius of the circle of contact is given by

$$a = 1.1 \{(1/2)Wgr[(1/E_1) + (1/E_2)]\}^{1/3},$$

where r is the radius of the sphere, E_1 and E_2 are the moduli of elasticity of the sphere and the surface, and W is the load.

Benjamin and Weaver assumed the forces on the tip are as shown in Figure 1, where F is the shearing force per unit area, W is the stylus load, r is the radius of the tip, P is analogous to a hydrostatic mean pressure, and a is the radius of the circle of contact, given as

$$a = (Wg/\pi P)^{1/2}.$$

Once full plasticity around the sphere is reached, the mean pressure over the contact area remains constant and equal to the indentation hardness. From this,

$$F = P \tan\theta = [a/(r^2-a^2)^{1/2}]\ P.$$

This shear force is a direct measure of adhesion, as it is assumed that it moves an atom of one layer from one equilibrium position to the next. If x is the distance between symmetrical equilibrium positions, then the height of the potential barrier is (1/2) F x, which is considered to be the energy of adhesion.

Butler, Stoddart, and Stuart (3), like Benjamin and Weaver, found that the scratch path involved deformation of both the film and the substrate. Load, film thickness, and relative physical properties of the film and substrate all affected the results. The scratch was usually a groove with a smooth center and raised sides. Often, a layer of the film remained in the center.

Two modes of film detachment were noted by these authors. The film could be cracked and partially detached after the stylus passed, perhaps due to failure of the film and interface to support the stresses

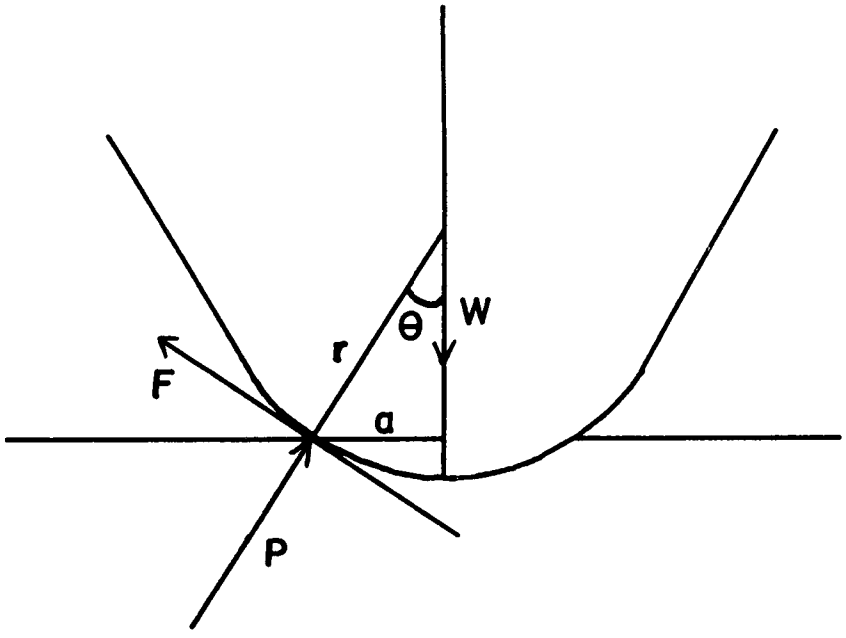


Figure 1. Forces at the lip of the stylus indentation as assumed by Benjamin and Weaver.

Source: Benjamin, P., and Weaver, C., "Measurement of Adhesion of Thin Films," Proc. Royal Soc. London A254 (1960) 163.

resulting from high substrate deformations. Alternately, the film became detached in an annulus around the stylus. Movement of the stylus left folds at the track edges, although the film sometimes did not tear or become carried away. In some cases, even when high loads distorted the system, no detachment was observed.

In this study, it was shown that separation of the film and substrate usually did not take place directly under the stylus but rather ahead of the stylus. This is in agreement with the theoretical results of Hamilton and Goodman (21), who, in 1966, obtained equations for the stress field due to a loaded spherical tip moving over a flat surface. Their yield parameter was defined using the von Mises criterion, which is the square root of the second invariant of the stress deviator, which, in Cartesian form is

$$J_2 = p_{xy}^2+p_{xz}^2+p_{yz}^2+(1/6)[(p_{yy}-p_{zz})^2+(p_{zz}-p_{xx})^2+(p_{xx}-p_{yy})^2].$$

Yield occurs when the square root of J_2 is equal to the material yield point in simple shear. The Cartesian stress components, p_{ij}, are derived in the paper. Evaluation of the above equation in the xz-plane (See Figures 2 and 3) for a coefficient of friction equal to zero reveals that the maximum yield parameter occurs on the centerline of the tip (z-axis) at a distance below the surface equal to 1/2 the circle of contact radius. As the coefficient of friction is increased, the maximum yield parameter moves toward the surface and in the positive x-direction, but a second maximum develops on the surface at a point behind the stylus and this second maximum supercedes the first for a coefficient of friction of 0.5.

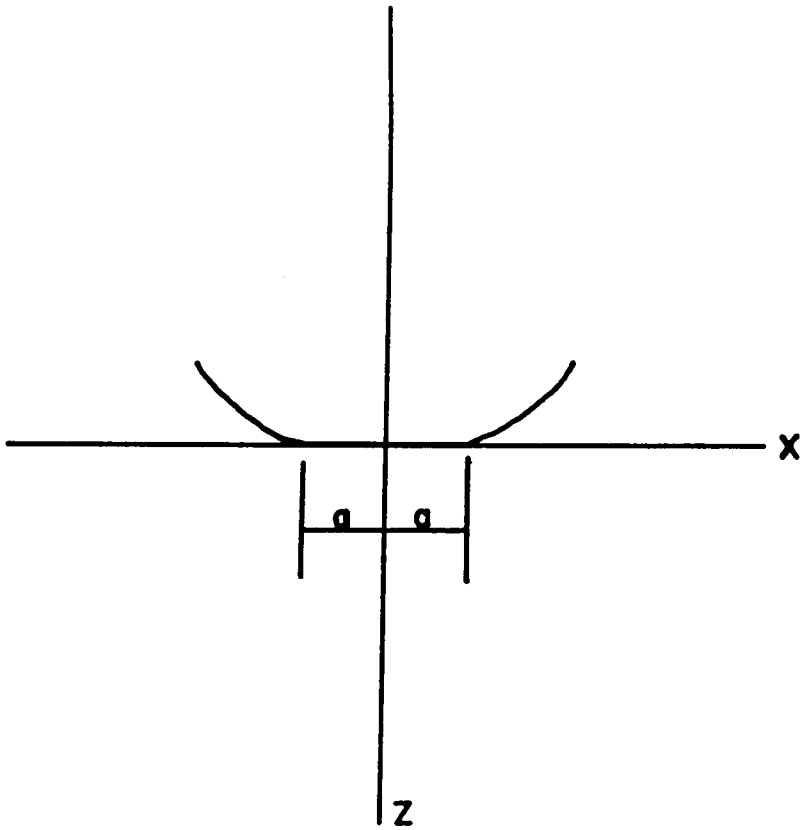


Figure 2. Schematic view of the stylus on the surface. The radius of the circle of contact is a and the stylus travels in the positive x-direction.

Source: Hamilton, G. M., and Goodman, L. E., "The Stress Field Created by a Circular Slidng Contact," J. Appl. Mech. 88 (1966) 71.

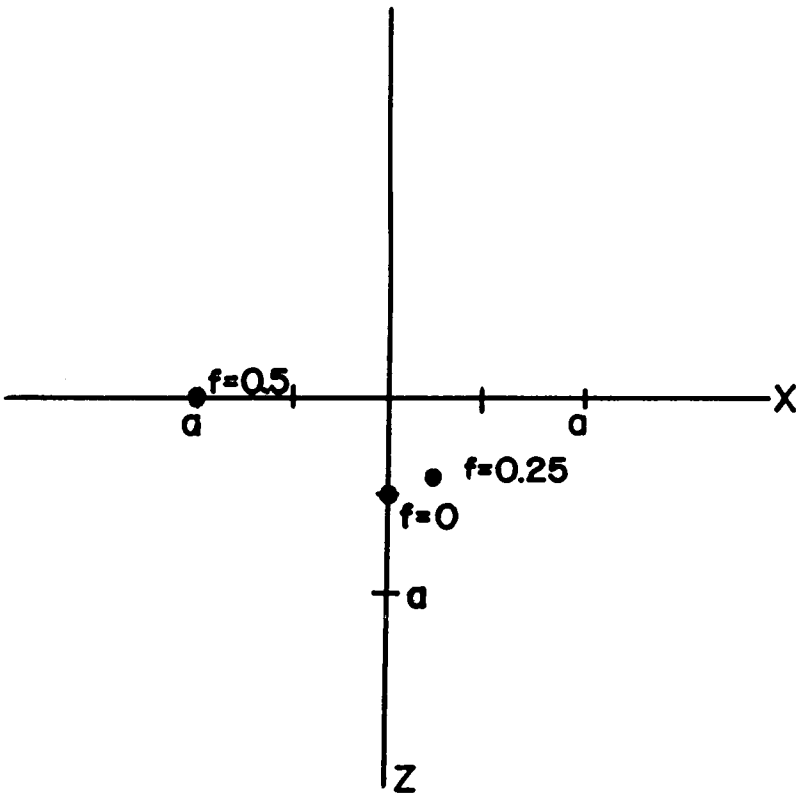


Figure 3. Points of maximum yield parameter below the stylus for various coefficients of friction. The stylus travels in the positive x-direction and the x-axis lies in the plane of the surface.

Source: Hamilton, G. M., and Goodman, L. E., "The Stress Field Created by a Circular Sliding Contact," J. Appl. Mech. 88 (1966) 71.

Laugier (7) suggested a model of the scratch test which included the coefficient of friction as a parameter. From stress equations of a hard sphere pressed against a flat surface developed by Hertz, Timoshenko and Goodier (25), and Hamilton and Goodman (21), he derived an expression for the total radial compressive stress acting at the leading edge of the moving indentor:

$$\sigma = (P/2\pi a^2)\{(4 + \nu_1)(3\pi f/8) - (1 - 2\nu_1)\}.$$

where ν_1 is Poisson's ratio for the flat surface, W is the normal load, a is the radius of contact, and f is the coefficient of friction. This total compressive stress is a combination of the radial tensile stress present at the lip of the indentation due to stretching of the film during deformation (See Figure 4) and the radial compressive stress generated by the movement of the stylus. From this expression for the radial stress, and assuming that the radius of the indentor, r, is much greater than the radius of the circle of contact, Laugier found the shear stress to be approximately

$$\tau \approx \sigma(a/r).$$

Letting $\nu_1 = 0.3$, the expression for the compressive stress becomes

$$\sigma \approx (Wg/2\pi a^2)(0.5f - 0.4).$$

The coefficient of friction, f, is seen to be very important: for a low coefficient of friction, the stress at the leading edge is tensile and the film will not "lift" from the substrate even if sufficient force to

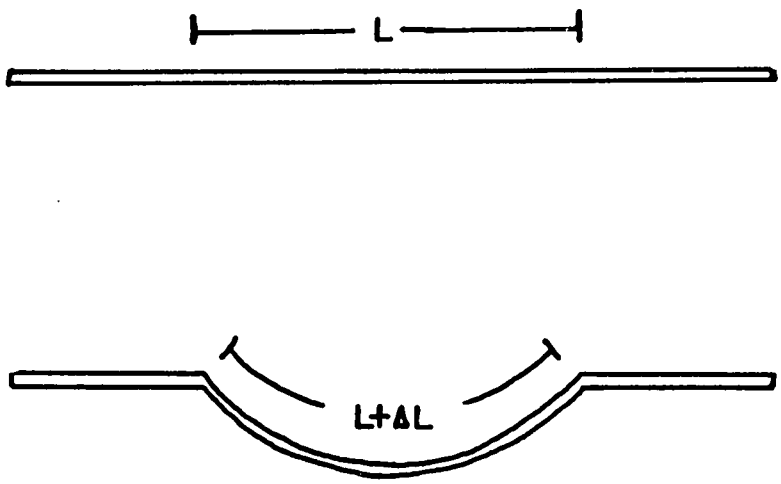


Figure 4. Stretching of the film during indentation. This stretching results in tensile stresses in the film under the stylus.

cause detachment has occurred. This would account for thinning of the film in the scratch path without material removal.

Laugier contended that his equations for conditions ahead of the stylus remain valid, in spite of their dependence on elastic parameters, since the onset of plasticity occurs at the trailing edge of the stylus for higher friction coefficients (from the analysis of Hamilton and Goodman, Figure 3).

In 1975, Weaver (5) admitted the scratching process was more complex than originally thought and tried to reconcile the observations with the previous successful use of the test. Since vacuum-deposited films are almost always in a state of tensile stress, he postulated that once the perimeter of the contact area is detached, the loosened edge of the film would tend to lift and peel away from the substrate, creating cracks. As the stylus advanced, it would push down the loosened edge, creating a hillock ahead of the stylus. If the stress is insufficient to produce crack extension, the loosened film would fold up in front of the stylus or be pushed aside until the stylus reached the end of the crack, at which point the process would be repeated. Evidence of this mechanism was found in electron micrographs which showed a periodic folding along the edges of the track, the spacing of which corresponded to the distance at which film was detached ahead of the stylus. Weaver attributed translucency without detachment to insufficient friction between the stylus and the film to transfer the force to the interface.

Other researchers (6,8) also found that the edges of the channel were subjected to gross plastic deformation and that high walls

developed. Extensive elastic recovery followed the passage of the stylus and this may explain why the scratches were wider and shallower than the stylus geometry would indicate (8). A typical scratch profile is shown in Figure 5. Cracking of the coating at the lip of the channel has been noted (8,13), as has been flaking of the coating ahead of the stylus (10). Detached fragments were pressed back onto the substrate in several cases (10,11). Micrographs from the work of Je, Gyarmati, and Naoumidis (11) clearly show cracking ahead of the moving stylus (See Figure 6) while a profile of the end revealed that the crack was not formed by bending (See Figure 7).

Takadoum, et. al. (26), studied the topography of scratches on films and observed continuous ridges along the edges of the channel and sometimes inside the channel; this was attributed to substantial plastic deformation of the surface. Perry and Pulker (23) also noted that the substrate used in their work was highly damaged during film removal.

Laeng and Steinmann (6) found Benjamin and Weaver's model to be invalid for the hard coatings used in their work. They included a dimensionless parameter

$$X = L/(r^2 H),$$

where L is the critical load, r is the tip radius, and H is the substrate hardness, in their analysis but found this to be, itself, dependent on the coating thickness and tip radius and thus failed to obtain quantitative values of the adhesion strength.

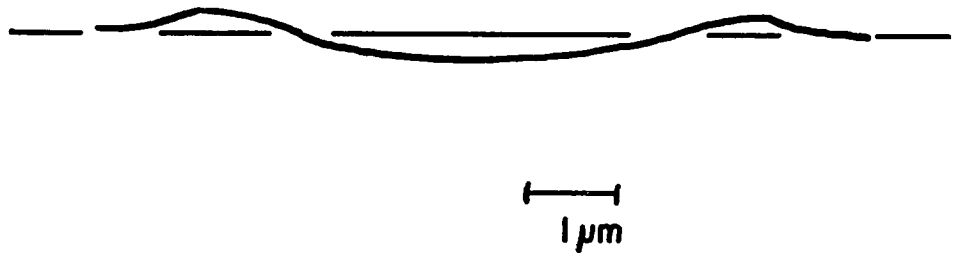


Figure 5. Typical scratch profile made with a 0.2-mm radius stylus tip.

Source: Laeng, P., and Steinmann, P. A., "Adhesion Testing of Hard CVD Coatings Using the Scratch Test," p. 723 in Proc. 8th Intern. Conf. on Chemical Vapor Deposition, John M. Blocher, Jr., Guy E. Vuillard, and Georg Wahl, eds., The Electrochemical Society, Inc., Pennington, NJ, 1981.

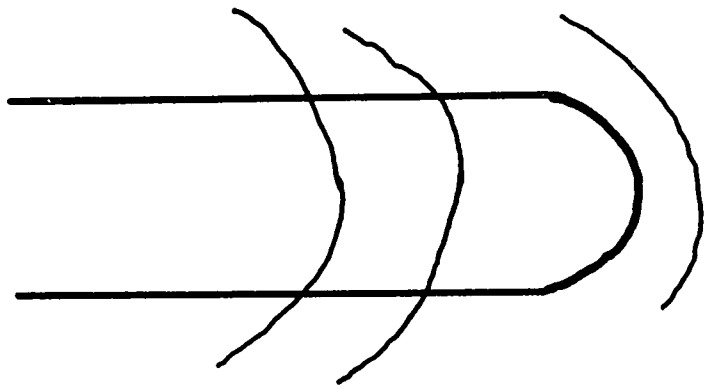


Figure 6. Schematic representation of the crack formed ahead of the stylus moving from left to right. Other cracks have been passed over by the stylus.

Source: Je, J. H., Gyarmati, E., and Naoumidis, A., "Scratch Adhesion Test of Reactively Sputtered TiN Coatings on a Soft Substrate," Thin Solid Films 136 (1986) 57.

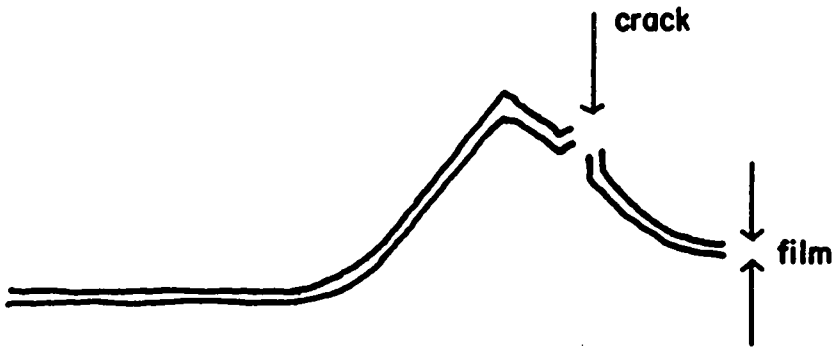


Figure 7. Height profile across the end of the channel showing the crack formed ahead of the stylus. Scratching is from left to right.

Source: Je, J. H., Gyarmati, E., and Naoumidis, A., "Scratch Adhesion Test of Reactively Sputtered TiN Coatings on a Soft Substrate," Thin Solid Films 136 (1986) 57.

In 1984, Laugier (27) proposed the following analysis of the scratch test using an energy description of the film removal. This method was suggested by the unsatisfactory fact that interfacial shearing, assumed by many to be responsible for de-adhesion when a critical load was reached, did not always result in film removal. Also, a necessary condition for coating removal ahead of the stylus is that the film must be under compression. Laugier concluded that, for ductile films, the material expands and lifts from the substrate to relieve the elastic energy stored in the compressively stressed region ahead of the stylus when this energy is sufficient to provide the work of adhesion and the work to deform the coating. This building up and relieving of stress produces folds along the edges of the scratch path. In the case of brittle materials, fragmentation or spalling of the coating occurs ahead of the stylus when the elastic energy is sufficient to provide the work of adhesion for detachment and work of fragmentation. It is assumed that, for both types of films, the work of adhesion is much more significant. Figure 8 shows the de-adhesion caused by energy stored ahead of the stylus. When this de-adhesion propagation was stopped, a cohesive crack formed between the detached and undetached material. Microcracking may occur as the stylus passes over the detached film.

The Acoustic Emission Test

Introduction and analysis. A scratch testing system can be equipped with an accelerometer, usually mounted just above the scratching stylus, that acts as an acoustic emission detector. Many

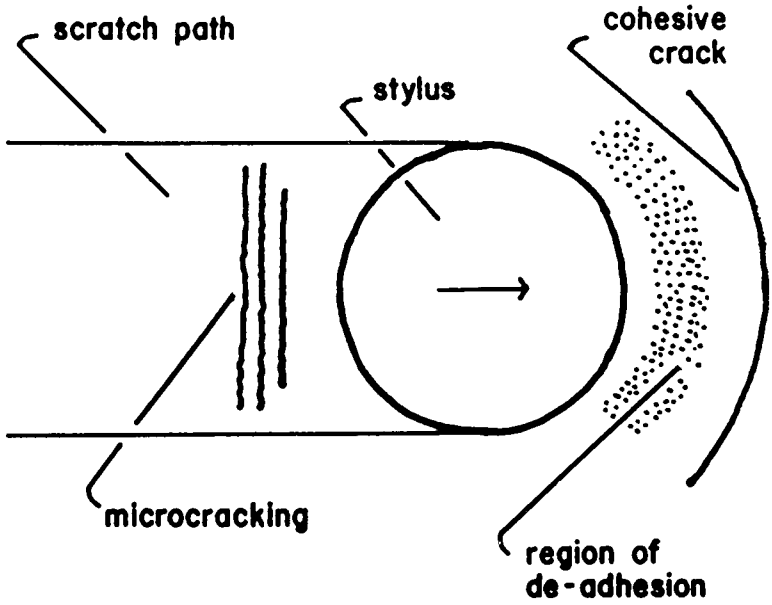


Figure 8. Model of failure by the scratch test. Elastic energy stored just ahead of the stylus causes de-adhesion. The de-adhesion propagates ahead of the stylus and is stopped by cohesive cracking of the film. Movement of the stylus on the detached film causes microcracking in the scratch path.

Source: Je, J. H., Gyarmati, E., and Naoumidis, A., "Scratch Adhesion Test of Reactively Sputtered TiN Coatings on a Soft Substrate," Thin Solid Films 136 (1986) 57.

researchers have reported good correlation between the acoustic emission signal and loss of film adhesion (6,8,10,11,13,18,22,28,29).

When a material undergoes deformation or fracture, some of the elastic energy induced by the local stresses can be released in the form of a stress wave (30,31,32,33). These stress waves produce small displacements which can be detected on the surface by a sensor. One theory for metals is that stress waves are generated from expanding plastic zones--the small area at the tip of a crack that undergoes plastic deformation due to stress concentration (30). Chanage in the amplitude distribution of the acoustic signal has been observed as a precursor to failure and it is believed that this is due to the beginning of local cleavage at the crack tip as instability begins (31). It has been observed for metals that acoustic emission only occurs when the previous maximum stress level is exceeded, indicating that the acoustic emission is dependent on plastic strain (30).

Acoustic emission signals are very dependent on the type of material, specimen size and geometry, previous stress in the specimen, and type of deformation processes (30). It has been noted that the data must have statistical strength to lead to correct conclusions (31).

A. A. Pollock (31) proposed a relationship between released energy and the amplitude of the acoustic emission. Referring to a model of a mechanical instability, for which the change in stored energy is proportional to the incremental deformation,

$$\Delta E \propto \Delta x,$$

the kinetic energy released is proportional to the instability,

$$\Delta E \propto I,$$

and therefore the instability is proportional to the incremental deformation,

$$I \propto \Delta x,$$

he devised an analogous description of an acoustic emission event. In the first stage, the crack tip disrupts the equilibrium of the local material stresses as it moves forward rapidly. In the second stage, propagation of a stress wave restores the mechanical equilibrium. Using this analogy, one would expect the amplitude of an emission to be proportional to the incremental specimen deformation:

$$A \propto \Delta x \text{ or } A = k_1 \Delta x.$$

According to classical wave theory, the energy should be proportional to the square of the amplitude:

$$\Delta E \propto A^2 \text{ or } \Delta E = k_2(k_1 \Delta x)^2 = k_3 \Delta x^2.$$

From this, the author concluded, and verified with experimental evidence, that the energy released as acoustic emission rises in proportion with the magnitude of the deformation event, rather than remaining a constant proportion of the total elastic strain energy:

$$\Delta E \propto \Delta x^2.$$

Thus, larger yields of acoustic emission result from larger deformation events.

Use in scratch testing. In 1971, Wilshaw and Rothwell (34) described an instrument, which they called an amychometer (from the Greek word for "scratch"), which measured both the normal force on a stylus and the acoustic emissions generated by microcracking of a glass surface as the stylus passed. They found an exact correspondence between the acoustic emissions and direct observation of the microcracks in an optical microscope.

Perry, et. al. (8,22) have investigated the relationship between acoustic emissions and loss of coating adhesion for several systems. From this data, it was concluded that acoustic emissions are associated with lateral crack propagation under a shear stress. No emissions were generated when the coating cracked perpendicular to the surface. Perry used his results as a measure of the load-bearing capacity of the coating, which could be due to cohesive and/or adhesive failure. Like Perry, Laeng and Steinmann (6) concluded from their work that there was no acoustic emission when the coating cracked perpendicular to the surface.

Perry (8) recorded acoustic emission as a function of stylus load and found more than a hundred-fold increase in the emission at the same load where microscopic examination revealed a change in surface morphology and some local loss. In spite of his good correlation between film damage and emissions, Perry cautioned that experience is needed in order

to attribute an increased acoustic signal to adhesive or cohesive loss or to film cracking.

Je, Gyarmati, and Naoumidis (11) compared an optical micrograph of a scratch track with the associated acoustic emissions. This data indicated that each crack formation results in an acoustic signal peak.

Use in other tests. Acoustic emission has also been used in adhesion tests other than scratch tests. In 1975, Curtis (32) used acoustic emissions derived from stressing adhesively bonded lap joints to conclude that (for the adhesives tested) more emissions will be released during failure for a weaker bond. Rooum and Rawlings (35) investigated layered automobile finishes and found that loss of adhesion, macro- and microcracking all resulted in acoustic emission for which there was good correlation between the emission and the degree of damage. Different failure mechanisms were characterized by emissions centered on specific amplitudes. For scale cracking during high temperature oxidation, Perkins and Meier (33) believed the source of the emissions to be cracks running parallel to the specimen surface, revealed by scanning electron microscopy. Bunnell, Crowe and Hart (36) found the monitoring of acoustic emission events to be extremely sensitive to surface damage effects in ceramics.

The Pull Test

Introduction. The pull test is a direct measure of the tensile force required to pull the film off normal to the substrate surface. Pins or studs of some kind are attached to the film surface and then

pulled off by a calibrated instrument such that the force of removal is known. The major difficulties of this method are in applying a truly normal force to the film, rather than a peeling force due to misalignment, and in the attachment of the pin to the film without grossly affecting the film under investigation or the interface between the film and the substrate (37). The limit of the test is the strength of the adhesive used to secure the pin to the film (9,12,38,39). Another difficulty is that failure can occur in a complex manner involving several of the interfaces in the system (pin/epoxy/film/substrate) rather than being confined to a single interface (36,40).

Consistent results by a number of researchers (38,39,40,41) as well as the straightforwardness of this method imply that it is a viable means of investigation. Varchenya and Upit (42) reported a mean spread of less than 20 percent for their data.

Variations in cement thickness and bond strength. In 1976, Jacobsson (38) analyzed the pull test in great detail and found the test to also be dependent on variations in cement thickness and homogeneity and on bonding strength variations. The stress will be higher than the average stress at a region where the cement is thinner. Since this higher stress is transmitted to the film, first failure will occur at the locations of minimum cement. In practical cases, no new equilibrium is reached after this first failure and thus total failure occurs. Using a simplified model with a uniform cement thickness distribution, Jacobsson and Kruse (43) showed that the force of adhesion measured for

a non-uniform cement thickness, F_B', is lower than the force of adhesion measured for a perfectly uniform cement thickness, F_B, and is approximately given by

$$F_B' = F_B [1-(1/2)(h_{max}-h_{min})/h_{min}],$$

where h_{max} and h_{min} are the maximum and minimum cement thicknesses.

In cases where the film adhesion strength varies, first failure may or may not lead to total failure, depending on the relative values of the maximum and minimum adhesive strengths (38).

Fracture energy analysis. Cannon, Fisher, and Evans (44) proposed the following analysis for the de-adhesion of a film under a normal tensile force using a fracture mechanics perspective. Cracks tend to extend normal to the maximum tensile stress and crack extension is driven by the strain energy release rate, G:

$$G = (-dW/dA + dU/dA),$$

where W and U are the external free energy and internal strain energy, respectively, and A is the crack area. One criterion is that extension of the crack occurs at a critical strain energy release rate, G_c. The crack extension path is modified by variations in growth resistance, including those due to prior crack extensions and external atmospheres. Variations in film thickness may also influence G_c, as the plastic zone size at the crack tip may be limited by the dimensions of the film. Experimentally, measurements and substrate cracking showed that maximum

values of the fracture energies, obtained for clean, well-bonded systems, are similar to those of the substrate.

The work of adhesion, W_{ad}, is the difference in equilibrium energies of the metal and ceramic surfaces created and the metal/ceramic interface destroyed and would be G_c if interfacial fracture were a reversible process. G_c exceeds W_{ad} due to the irreversible behavior of crack growth and any plasticity in the system. Fracture energies can be much lower than the maximum values, however, due to poor bonding between the film and the substrate.

Ion Beam Mixing

Introduction

Ion implantation originated in the early 1960's when semiconductor researchers began using beams of energetic ions to control the number and depth of the dopant atoms (45). The technique had previously been used by physicists and nuclear chemists in their fundamental research into the nature of crystals and the changes caused by atomic collisions. The high energy dopant ions originate at one end of an accelerator and are driven and focused by an electric field until they enter the target chamber and collide with the target material (45). In ion beam mixing, the ion energies are adjusted such that most of the damage is done at the interface. Atoms from the film may be forward sputtered into the substrate and atoms from the substrate may be back-sputtered into the film. This transfer creates a transition layer at the interface (39), eliminating the narrow interface through which a fracture may more

easily propagate. Basta (46) referred to this process as "stitching" the coating to the substrate. In some cases, however, an abrupt interface remains (47).

Effect on Adhesion

Hondros (48) attempted to explain the increase in adhesion strength after ion beam mixing with a discussion of the thermodynamic work of adhesion and the surface free energy of materials. He asserted that a process, such as ion beam mixing that reduces the interfacial energy, increases the work of adhesion.

Many researchers (16,19,47,49,50,51,52,53) have reported an improvement in film adhesion as the result of ion beam mixing. However, the apparent increase in adhesion may not be due solely to better adhesion. Ion beam modification can increase the hardness of the surface (54,55,56) and decrease the frictional forces (16,57), which may be important parameters depending on the mode of testing.

CHAPTER III

EXPERIMENTAL PROCEDURE

Substrate Materials

Four different substrate materials were used in this study.

Sapphire (Al_2O_3) single crystals, 25.4 mm in diameter and 1.0 mm thick, were supplied by Crystal Systems, Inc. These crystals had been cut to within 2 degrees of the basal plane and polished by the supplier. The crystals were annealed for 120 h at 1450 to 1500°C in air to remove any residual defects. Each crystal was cut into quarters such that the pieces could fit into the ion beam accelerator chamber.

Glass plates 25.4 by 12.7 mm were cut from standard glass microscope slides. These slides had been precleaned and displayed few scratches when viewed optically.

Bars (3 × 6 × 52 mm) of reaction bonded silicon nitride (RBN) and sintered alpha silicon carbide (SASC) were supplied by Garrett Gas Turbine Company, Phoenix, AZ. After being polished to a metallographic finish, the bars were coated with either 15 or 30 nm of aluminum or zirconium and ion beam mixed to various doses by personnel of the Solid State Division of Oak Ridge National Laboratory. These specimens were then used for adhesion testing.

Substrate Cleaning Procedure

The following cleaning procedure was utilized for the sapphire and glass substrates preceding film deposition:

1. Ultrasonically cleaned in Micro laboratory cleaning solution (15 min for each side);
2. Rinsed thoroughly in distilled water;
3. Ultrasonically cleaned in acetone (10 min for each side);
4. Rinsed thoroughly in distilled water;
5. Ultrasonically cleaned in ethyl or isopropyl alcohol (5 min for each side);
6. Rinsed with alcohol;
7. Oven dried at 100°C.

This technique, however, removed the 30 nm aluminum film on the RBN and SASC and was therefore not used on any of the other specimens that already had a film. Details are provided in a following section.

Film Deposition

Two apparatus were utilized for the film deposition.

The first system was a NRC Vacuum Coater. This consisted of a 10.16-cm diameter diffusion pump, 35-centimeter diameter, 60-cm high bell jar, and used electrical resistance to heat either a tungsten basket filled with the deposition metal or a tungsten wire coated with the material to be deposited. Lowest vacuum pressures were approximately 1.1×10^{-3} Pa with most depositions taking place at a base pressure of about 2.7×10^{-2} Pa. Film thickness was judged optically through the bell jar.

The second system was an Airco Temescal tri-gun electron beam evaporation system with three separate and independent electron beam

sources and a 15.2-cm diameter diffusion pump. In this system, bulk material was heated by an electron beam in a water-cooled copper crucible while the substrate specimen remained shielded by a movable shutter. Deposition rate and film thickness were monitored by a quartz crystal in the chamber. This crystal provided a feedback system to adjust the power to maintain the deposition rate and to shut the power off when the correct thickness had been attained. After the deposition rate reached a preset value of 1 nm/s, the substrate was exposed and the deposition proceeded under electronic control. Base pressures were approximately 1.3×10^{-4} Pa while pressures during deposition ranged up to 1.3×10^{-3} Pa. Although the substrates were not intentionally heated, radiant heating of the chamber raised the substrate temperatures to approximately 50°C.

The diagram in Figure 9 shows the electron beam power as a function of time. During the rise and soak times, the bulk deposition material and the chamber were heated to the deposition temperatures to degas the melt and drive off any surface oxides. The predeposit time allowed the deposition rate to reach the preset value before the specimen substrate was exposed.

Films of chromium, zirconium, nickel, and aluminum were deposited by one of these methods. Thicknesses of 100, 200, and 500 nm were deposited.

Specimen Characterization

Hardness tests were performed using a Leitz Miniload Hardness Tester to determine the Vickers hardness. Substrate hardnesses were

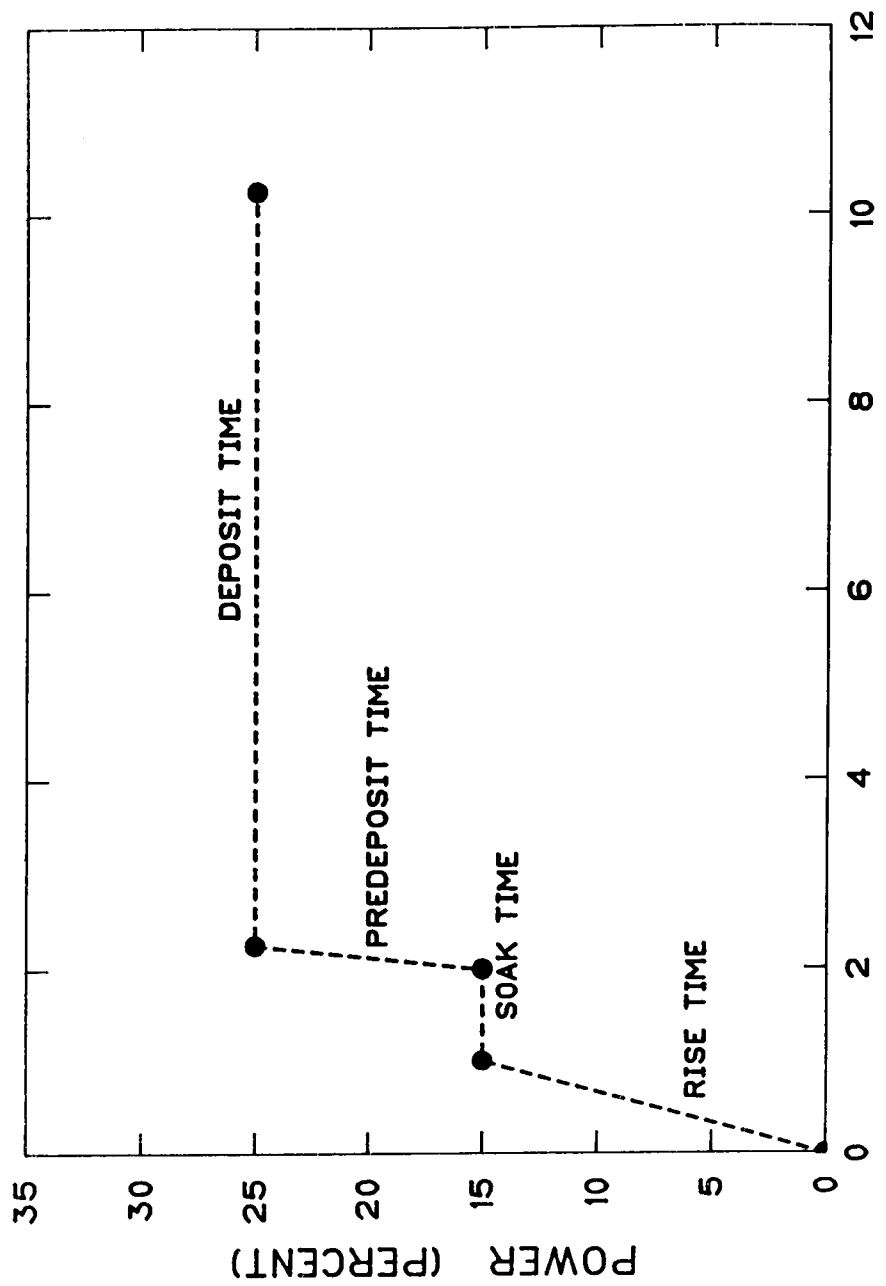


Figure 9. Electron beam power as a function of time for the deposition of the zirconium film.

found using a 100-g load for 30 s. Film/substrate hardnesses were found using both a 100-g load for 30 s and using a load such that the indentation depths were of the order of the scratches made during scratch testing.

Substrate and film surface characterizations were made using a Tencor Alpha Step 200 profilometer fitted with a 0.22 μm radius diamond stylus under a load of 2 to 4 mg. Scan lengths of 400 and 2000 μm were made. Arithmetic average surface roughness values, calculated by the instrument (ANSI Standard B46.1–1978, graphically determined), were taken as a measure of the surface roughness of both the substrate and film and the step height at the edge of the film was used as a measure of the film thickness.

Scratch Test

The scratch tester used for this project is shown in Figure 10. It consisted primarily of a balanced lever arm with a diamond stylus and a load platform directly above the stylus. The stylus, a spherical diamond or steel penetrator for Rockwell Hardness testing, was a separate piece such that its extension below the load platform was adjustable. To begin testing, the lever arm was exactly balanced in the horizontal position with the tip of the stylus just touching the specimen surface when the specimen was mounted on the movable stage below. The stylus and load platform mounted on the lever arm were rigidly attached to a strain gage such that all tangential (horizontal) forces on the stylus were measured. The strain gage was adjusted to read zero

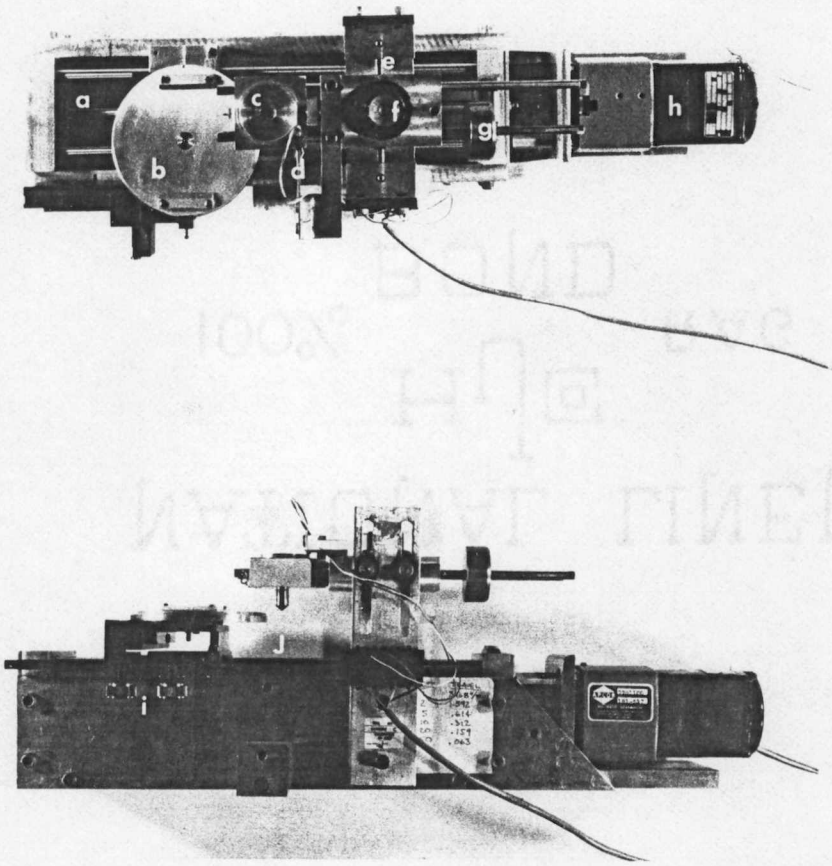


Figure 10. The scratch tester. The following parts are labeled: (a) drive shaft; (b) movable stage; (c) load platform; (d) strain gage; (e) axis of lever arm rotation; (f) carpenter's level; (g) balance weight; (h) motor; (i) horizontal plane adjusters for stage; (j) stylus. Actual length: 50 cm.

in the no load configuration. A load was then placed on the load platform. The stage with the specimen rigidly mounted was moved under the stylus at a constant speed of 1.6 mm/min by a gear ratio motor. The signal from the strain gage was outputted to an analog recorder that plotted tangential force on the stylus versus time (which corresponded to length of the scratch). In each case, the specimen was aligned so that the scratch began at least 0.5 mm before the edge of the film and continued approximately 1 mm across the film.

Although there existed some vibrations of the system caused by the gear ratio drive motor, unpredictable vibrations were eliminated by operating the equipment on a Vibraplane inertia isolation table.

Acoustic Emission Test

In the current investigation, an accelerometer was mounted to the side of the stylus on the load platform. This was then connected to a shock amplifier and the amplifier connected to a strip chart recorder. More than fifty scratches were made with varying film materials, normal loads, chart sensitivities and speeds, amplifier sensitivities and frequency filters. However, no patterns emerged that signified loss of adhesion; in fact, no difference could be detected between when the stylus was running on the bare substrate and when it crossed onto the film. It is suspected that whatever specimen emissions might have occurred were overshadowed by those of the drive motor, which could not be adequately isolated from the system.

Pull Test

The pull testing was done using a Sebastian I Adherence Tester manufactured by the Quad Group. In this test, pre-epoxied bonding pins supplied by the Quad Group were attached to the film surface by clips and then oven cured. Much experimentation was done to determine the cure cycle that would deliver the maximum epoxy strength and adherence to both the film and the pin. This was found to be a 0.5-h temperature ramp to 150°C, 1.5 h at 150°C, and then oven cooled to room temperature. The specimens were then allowed to sit for at room temperature for at least 24 h before testing. The tensile stress required to remove the pin was indicated on a digital display and the accuracy was specified as being ±10 percent. An analog recorder was also attached to the equipment so that a force versus time plot was also generated, thus allowing the calculation of the energy to failure.

Other commercial epoxies were also used in conjunction with the Sebastian Adherence Tester studs that did not have a pre-coat of epoxy. None of these had a greater bonding strength than the pre-epoxied pins and thus no data is reported for these trials.

Ion Beam Mixing

The ion beam mixing was performed on all of the sapphire and glass specimens using the Oak Ridge National Laboratory 5 MeV Van de Graaff accelerator supplying Fe+ ions at 1 MeV to a fluence of 1×10^{17} ions/cm^2. A portion of each specimen was masked to preserve a virgin region.

The computer code E-DEP-1 (version 5) supplied by the Naval Research Laboratory (58) was used to calculate the distribution of energy deposited into elastic collisions as a function of heavy ion penetration depth into an amorphous material. This data gave assurance that the ion beam was penetrating the film and mixing was occurring in the interfacial region.

CHAPTER IV

RESULTS AND DISCUSSIONS

The Scratch Test

The scratching of a thin ductile film on a brittle substrate is a very complex phenomenon.

The final judgement of the integrity of the film in this study was based on the transmission of light through the specimen: since the substrate was transparent and the film opaque, transmitted light signified an absence of the film. There are drawbacks to this method, as noted in the literature review, since ductile films may be thinned to transparency by sideways extrusion and some films, while non-adherent, may be pressed back into the scratch path under the passing stylus. An attempt was made to distinguish between film loss and film thinning. Also, the total stress state of the film, including inherent stresses developed during growth and thermal cycling, and applied stresses due to the normal loading and friction, may be such as to prevent the film from pulling away from the substrate and thus de-adhesion will not be detected. Some judgement must be used in defining film loss. Small portions of film removed may be due to flaws (either inherent or created during handling) and may or may not be considered important, depending on the purpose of the experiment. In this work, only regular or continuous, easily detected stripping was considered significant.

Systems Analyzed

Aluminum films on glass. Difficulty in the analysis of very adherent films led to the use of aluminum films on glass substrates since this system proved to have very low adherence. The films did not pass the tape test (were removed by plastic tape) and optical microscopy using a light source below the transparent substrate revealed the critical load, as defined as that normal load at which the film is stripped from the substrate, as being less than 1 g (0.0098 N). The aluminum films were 120 nm thick and had an average arithmetic surface roughness of 5 nm. Although no noticeable differences in the film surfaces were found from surface profilometry, large differences in the coefficients of friction under the stylus, at the same normal load, were recorded.

Nickel and chromium films on sapphire. Chromium was chosen as a film material based on some earlier promising results. Hondros (48) observed that nickel had relatively poor adhesion to sapphire and it was felt that this system had good promise for measurable improvement by ion beam mixing. Nickel films and chromium films on sapphire substrates proved to be much more adherent than the aluminum films to glass. Typical critical loads, although inconsistent, were of the order of 50 g. These films were approximately 200 nm thick.

Zirconium films on sapphire. Two of the zirconium films were extremely adherent to their sapphire substrates. Even scratches made under a 300-g load did not cause de-adhesion of the film. Scratches made using normal loads less than 150 g were not visible in an optical

microscope at a magnification of 40X. Other scratches were barely visible even under a magnification of 700X. However, another of these specimens had relatively poor adherence: the critical load for it was approximately 10 g.

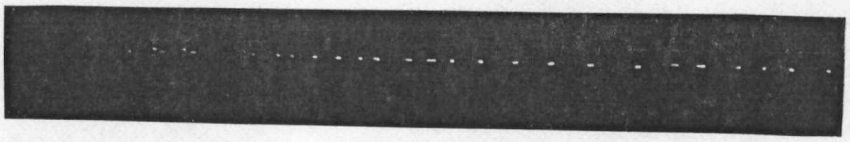
Scratch Characteristics

System vibrations and noise. System vibrations due to the gear ratio drive motor were apparent for the very low normal loads used to investigate the aluminum/glass systems. Figure 11 shows a scratch made under a 0.45-g normal load but at a speed 50 times faster than used for actual testing to exaggerate the skipping effect. Figure 12 shows a similar pattern obtained during an actual test under a normal load of 2 g. This skipping was not apparent at higher loads because the change in loading due to this vibration is such a small percentage of the total loading for the more heavily loaded scratches.

Noise generated by the strain gage, strain gage analyzer, analog recorder, and connecting cables lowered the resolution of the tangential force measurement. The lack of sensitivity to very subtle changes in the tangential force may have prevented a more accurate description of the stress state of the film.

Due to the combined effects of system vibrations and noise, the scratch test can be considered to have a lower limit. Adhesion levels below this limit cannot be adequately measured.

Characteristics of the scratch path. Typical scratch profiles are shown in Figure 13. The ridges beside the path may or may not be

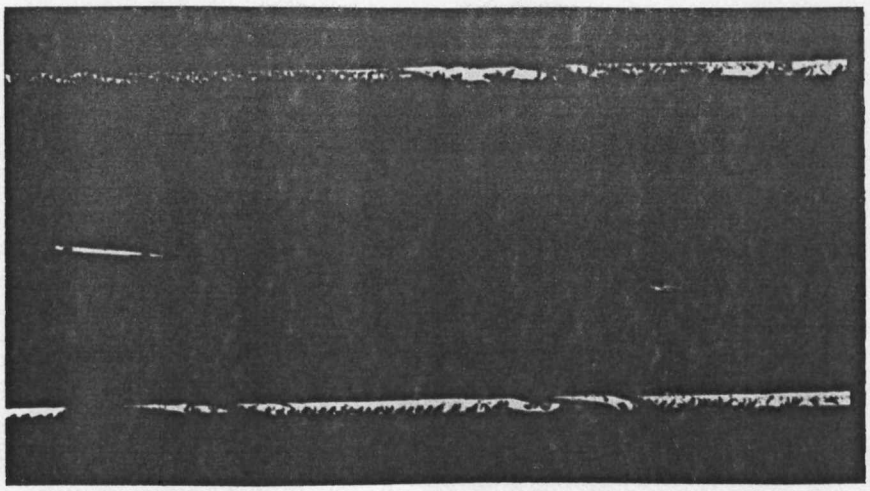


(a) Transmitted light. 42X.

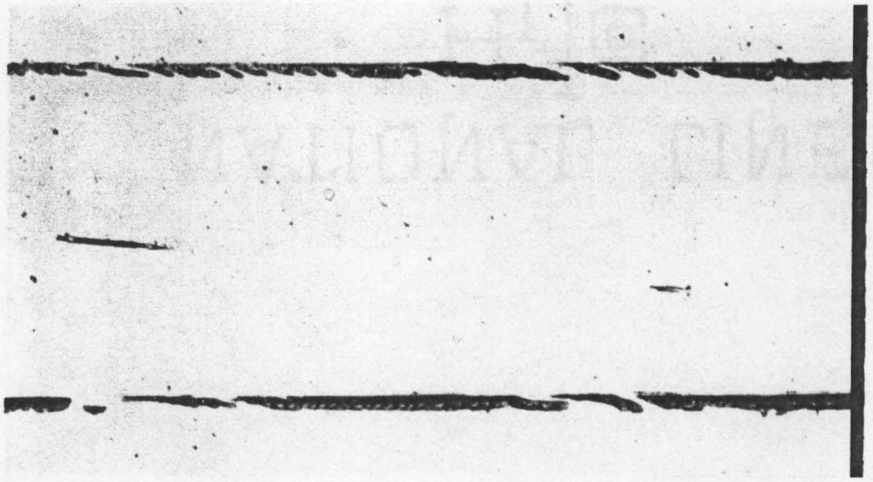


(b) Reflected light. 450X.

Figure 11. Stylus skipping caused by system vibrations. Scratch made on aluminum/glass system under a normal load of 0.45 g. The speed of the stylus travel was increased to exaggerate the skipping effect. Scratch direction is from left to right.



(a) Transmitted light. 68X.

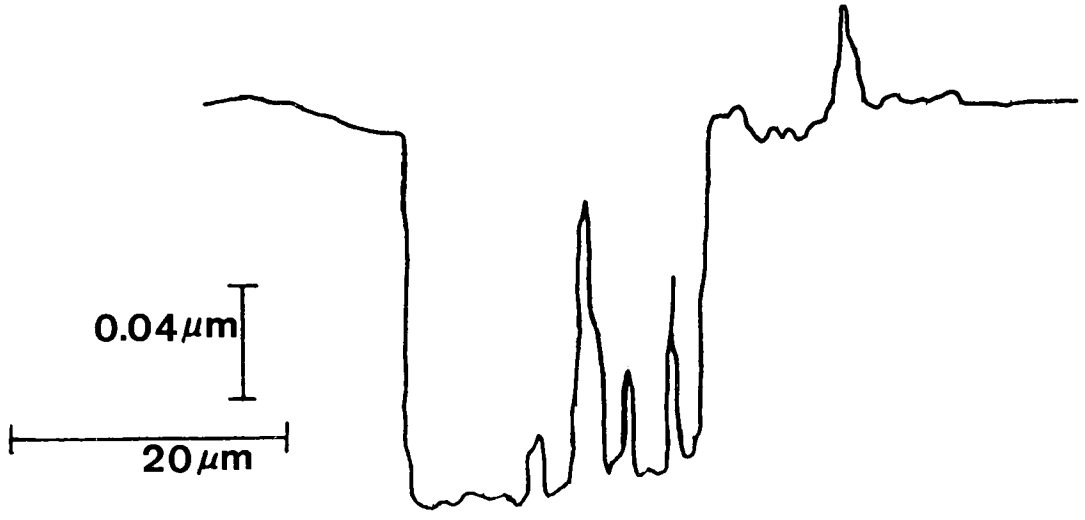


(b) Reflected light. 68X.

Figure 12. Scratch made on aluminum/glass system under a normal load of 2.0 g. Scratch direction is from left to right.



(a) Nickel film on sapphire.



(b) Aluminum film on glass.

Figure 13. Typical scratch profiles.

present, depending on the mode of deformation. Ridges in the center of the track are quite common.

The scratch path is, in general, neither uniform nor symmetrical, even at loads higher than the critical loads. This is evident from both the profiles of Figure 13 and the micrographs of Figures 14, 15, and 16. For the aluminum/glass systems, some of the film material pushed out of the path of the stylus remained attached to the side of the channel. These pileups often immediately preceded a section of narrow track or a skipped region, indicating that material had piled up ahead of the stylus, sufficiently increasing the resistance to motion to cause the stylus to rise onto the film surface in order to keep on moving. Many of these flakes were not removed in an ultrasonic bath, denoting that the film was not broken from the side of the channel. Figures 17 and 18 show two such regions, before and after ultrasonic cleaning. It is not known what contribution the system vibrations made to this skipping. The irregularity, however, implied that the vibrations were not the most significant aspect. Figure 19 shows the full length of the scratches in Figures 17 and 18, and it can be seen that the skipping is not regular.

Thinning of the film under the stylus was particularly apparent for the zirconium films on sapphire. This may be due to a stress state unfavorable to film removal, even if de-adhesion has occurred (7). Film thinning under both 10 and 200 g normal loads can be seen in Figure 20.

Occasionally, significant scratching was initiated by the presence of a surface flaw. This is illustrated clearly in Figure 21.

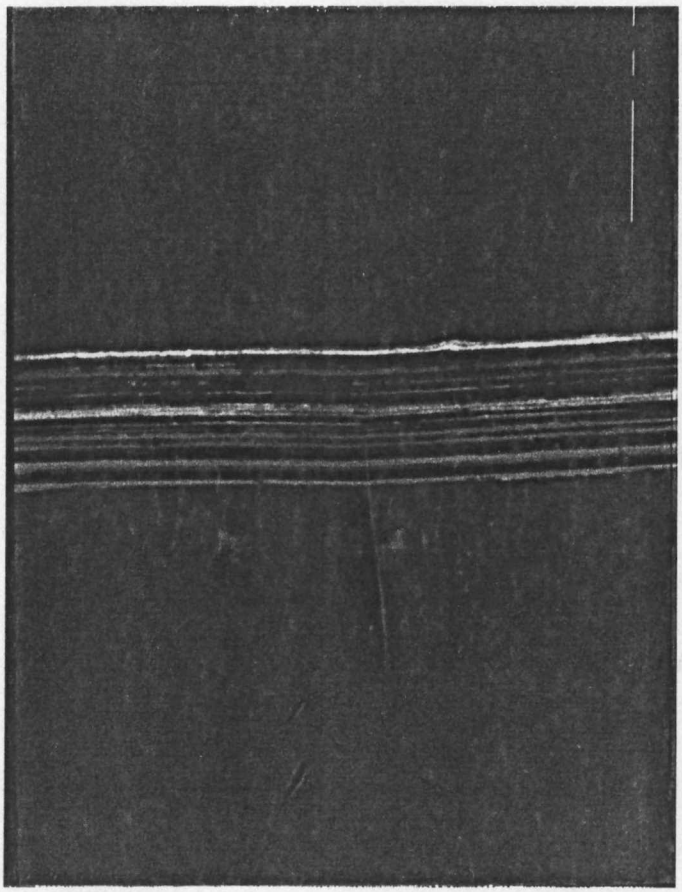


Figure 14. Scratch made on zirconium/sapphire specimen under a normal load of 30 g. Scratch direction is from left to right. Scanning electron micrograph, 1600X.

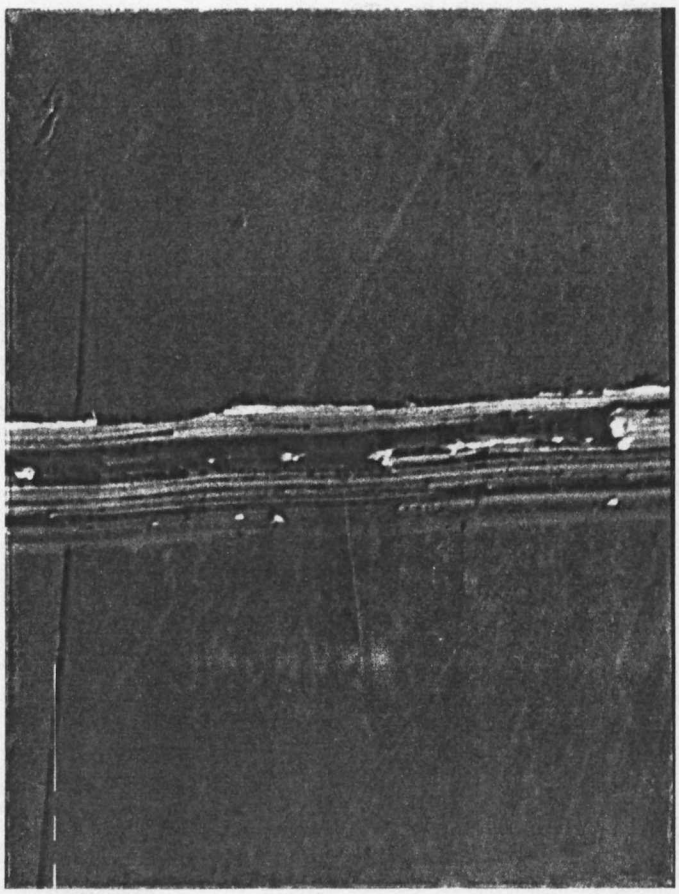


Figure 15. Scratch made on zirconium/sapphire specimen under a normal load of 40 g. Scratch direction is from left to right. Scanning electron micrograph, 1650X.

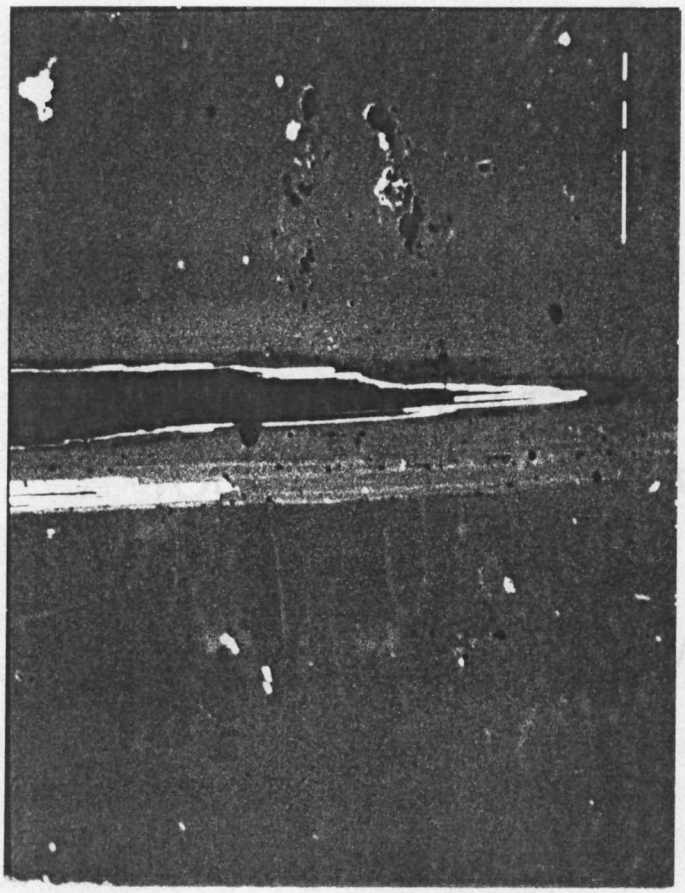
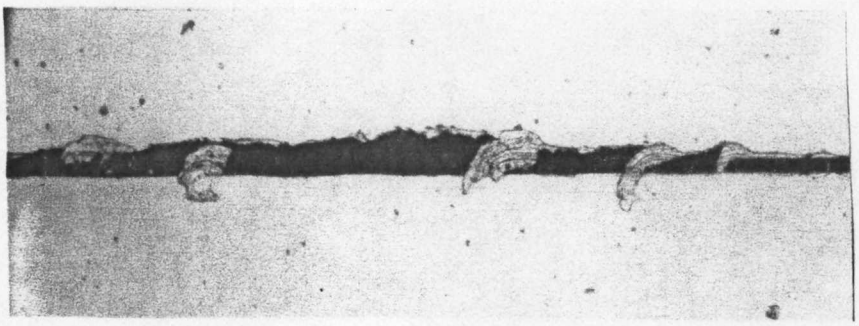
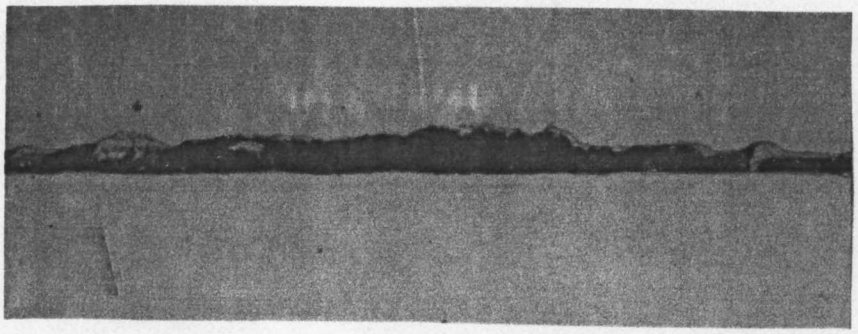


Figure 16. Scratch made on nickel/sapphire specimen under a normal load of 150 g. The white streaks signify film removal. Scratch direction is from left to right. Scanning electron micrograph, 1430X.

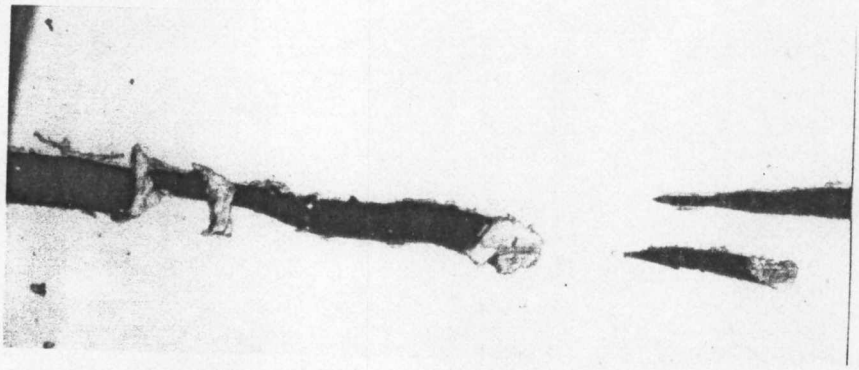


(a) Before ultrasonic cleaning. 450X.

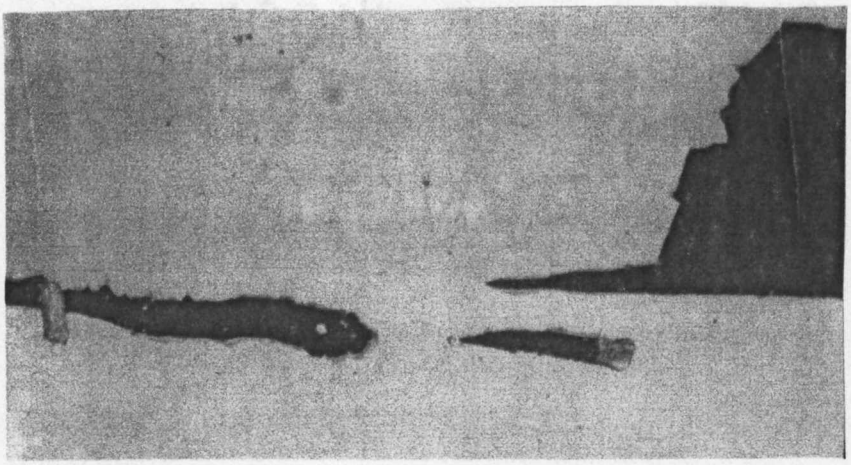


(b) After ultrasonic cleaning. 450X.

Figure 17. Scratches made on aluminum/glass specimen under a normal load of 0.45 g. Scratch direction is from left to right.



(a) Before ultrasonic cleaning. 450X.



(b) After ultrasonic cleaning. 450X.

Figure 18. Scratches made on aluminum/glass specimen under a normal load of 1.0 g. Scratch direction is from left to right.

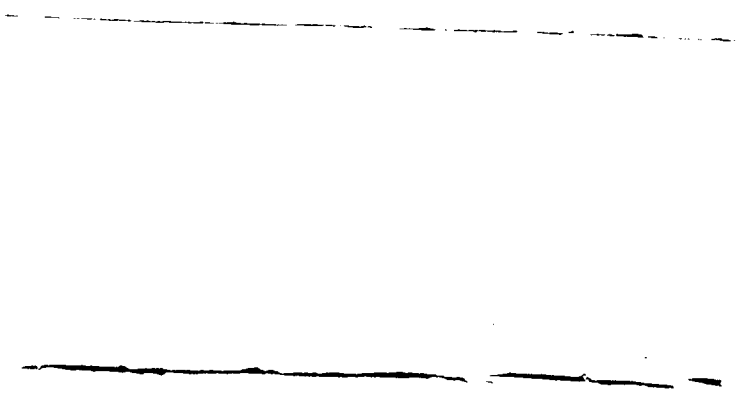


Figure 19. Full length view of scratches in Figures 17 and 18 before ultrasonic cleaning. Scratch direction is from left to right. 42X.

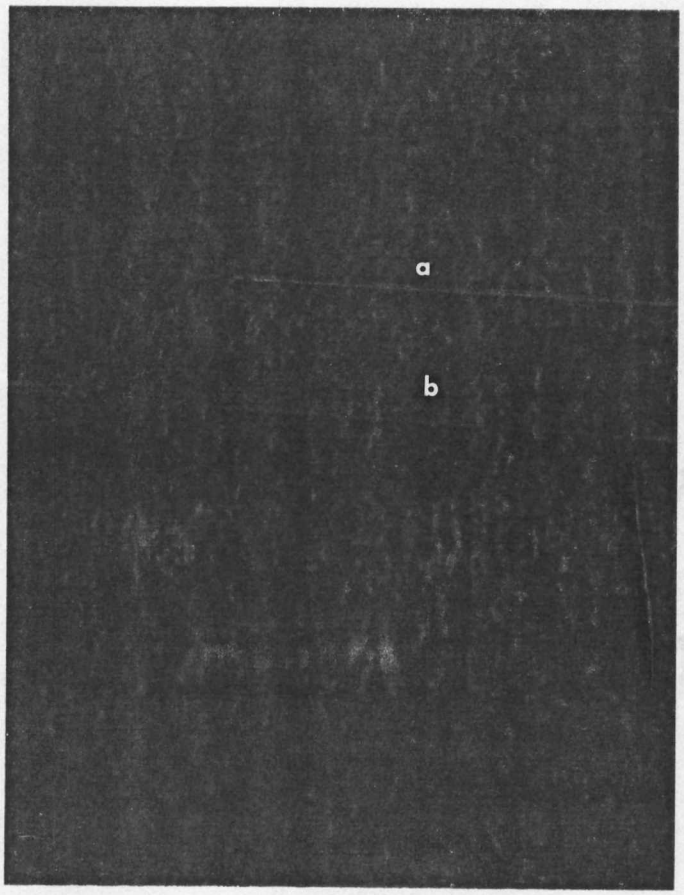


Figure 20. Thinning of zirconium film under normal stylus loads of (a) 10 g and (b) 200 g. 128X.

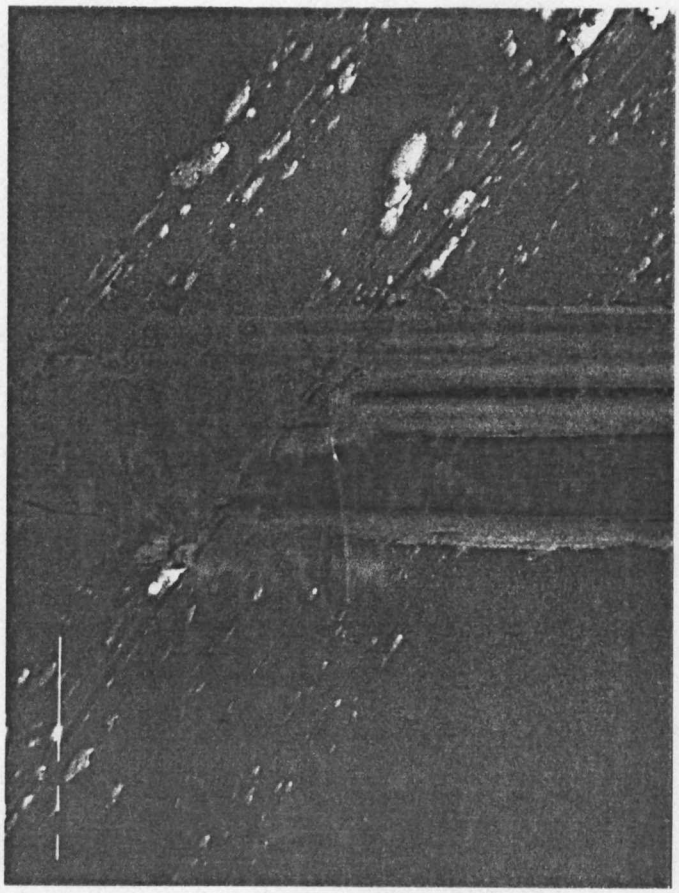


Figure 21. Effect of surface flaw on scratching of zirconium/sapphire system. Scratch direction is from left to right. Scanning electron micrograph, 1600X.

Deformation modes. Comparison of the scratches made by the diamond stylus on the chromium and nickel films on sapphire substrates revealed a significant difference in the deformation modes. Transverse profiles of the scratches made on nickel/sapphire systems showed hillocks all along the edge of the scratch channel (See Figure 22). This is indicative of ductile extrusion under the stylus. Scratches made on chromium/sapphire systems, however, showed no evidence of extrusion in either profiles or micrographs (See Figures 23 and 24). Figure 24 does show some material along the side of the channel but the irregularity of its occurrence indicates that the film was broken and then pushed aside by the passing stylus rather than extruded from underneath the stylus.

The scratches in Figure 25 were made on an ion beam mixed zirconium/sapphire system. These show a compressive failure in the form of "bubbles" to the side of the scratch path. The scratch path itself has only been thinned: film removal occurred only in the "popped out" regions to the side of the channel. Since evaporated films are almost always in a state of tension, the compressive stresses were most likely generated ahead of the moving stylus in both the film and the substrate. Also, if it were the film alone that failed, de-adhesion would have initiated immediately next to the path where the film was weakened, rather than away from the track as it appears to have done.

The analysis of Hamilton and Goodman (21) describing the tensile stresses behind the moving stylus is supported by Figure 26. Theoretical lines of constant tensile stress acting in the plane of the surface are shown in Figure 27 for a coefficient of friction of 0.25.

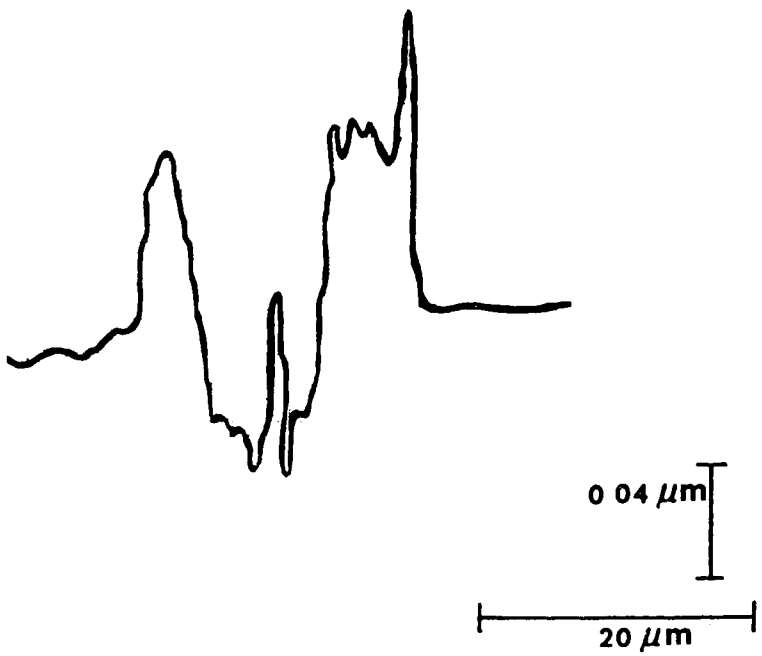


Figure 22. Transverse profile of a scratch showing ductile extrusion of nickel film on a sapphire substrate.

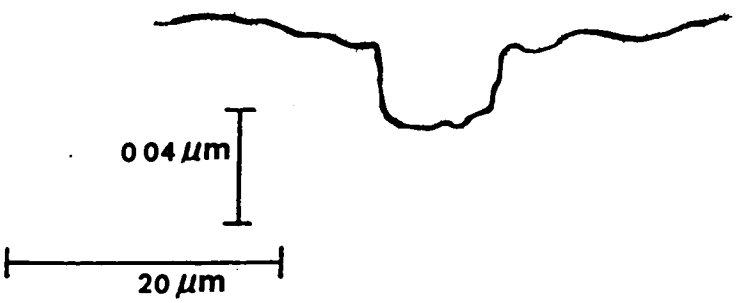


Figure 23. Transverse profile of a scratch showing absence of ductile extrusion of a chromium film on a sapphire substrate.

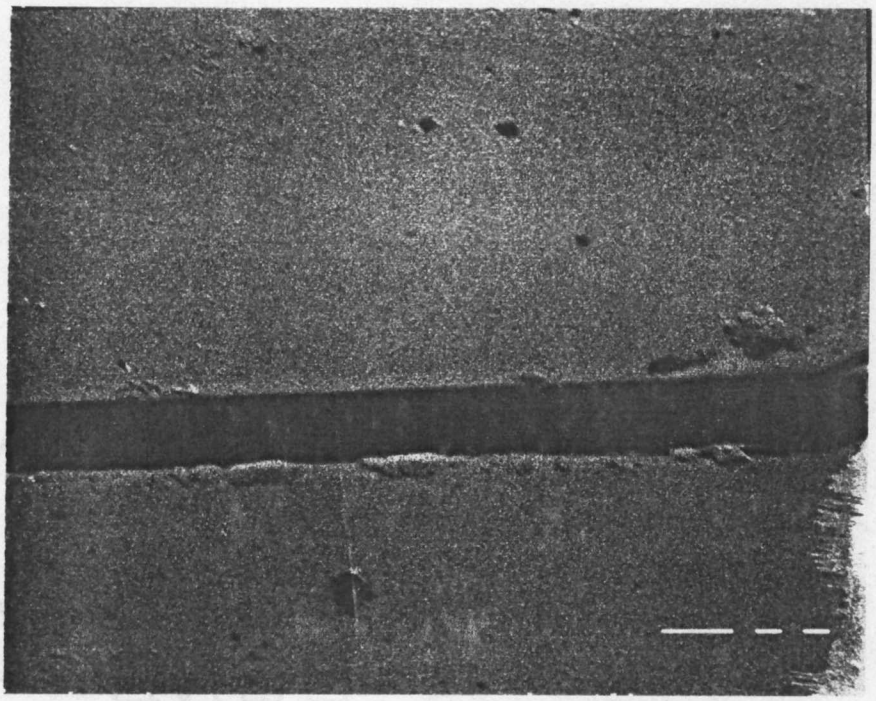
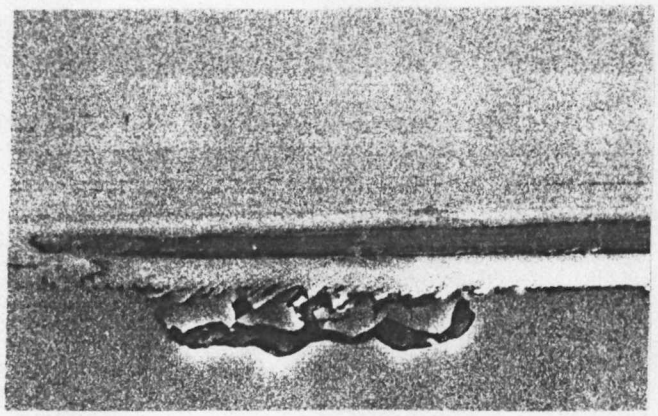
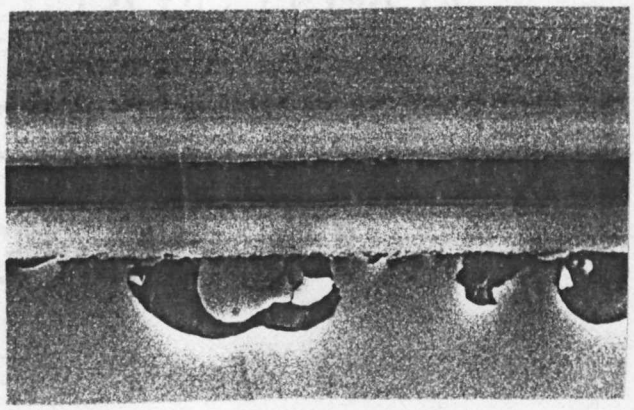


Figure 24. Scanning electron micrograph of a 250-g normal load scratch on a chromium/sapphire specimen. Scratch direction is from left to right. 1000X.

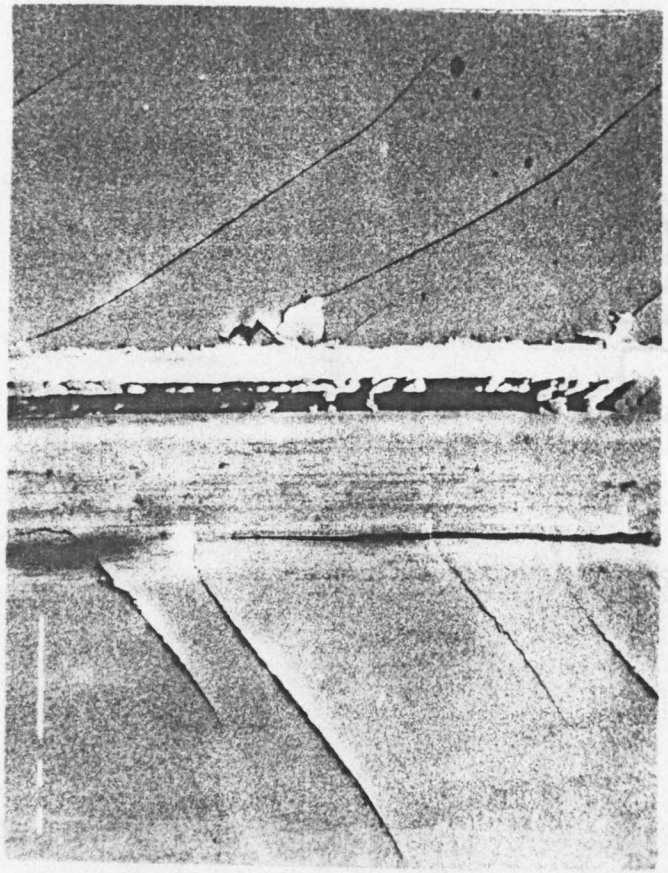


(a) Scanning electron micrograph, 1600X.

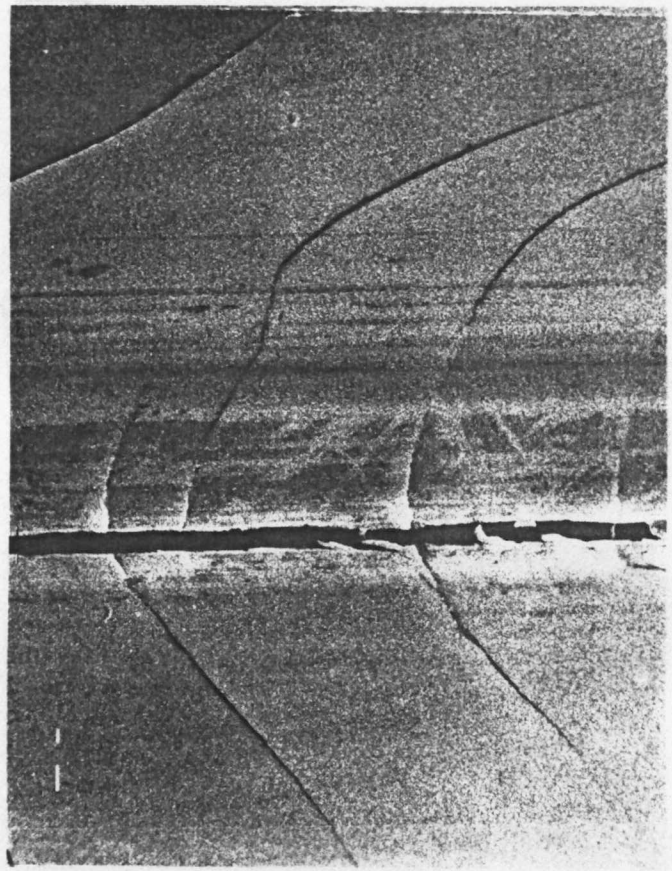


(b) Scanning electron micrograph, 1700X.

Figure 25. Two regions of compressive failure caused by a 450-g normal load scratch on a zirconium/sapphire specimen. Scratch direction is from left to right.



(a) Scanning electron micrograph, 1600X.



(b) Scanning electron micrograph, 1900X.

Figure 26. Tensile failure behind the moving stylus caused by a 400-g normal load on a zirconium/sapphire specimen. Scratch direction is from left to right.

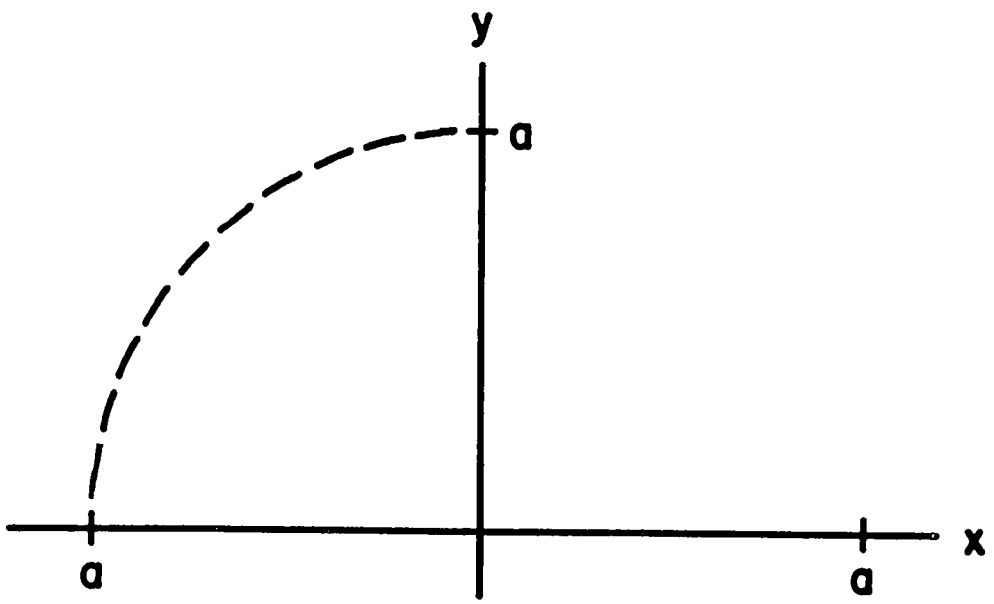


Figure 27. Theoretical line of constant maximum tensile stress acting in the plane of the surface for a friction coefficient of 0.25. The stylus moves in the positive x-direction and a is the radius of the circle of contact.

Source: Hamilton, G. M., and Goodman, L. E., "The Stress Field Created by a Circular Sliding Contact," J. Appl. Mech. 88 (1966) 371.

The line of constant maximum tensile stress lies in almost an identical location for a friction coefficient of 0.50. Comparison of Figures 26 and 27 reveals that the cracks of Figure 26 almost exactly propagate along the theoretical lines of maximum tensile stress. The dark lanes in the scratch paths of the micrographs are regions stripped of the film. It is interesting to note the lack of symmetry in the scratch path and that the cleared portion actually changes sides (both micrographs of Figure 26 are from the same track).

The systems illustrated in Figures 25 and 26 were both from the same zirconium/sapphire specimen but the failure modes were very different: the first, in the ion beam mixed region, was a compressive failure ahead of the moving stylus, whereas the second, in the unmixed region, was a tensile failure behind the stylus. The results of these tests cannot be quantitatively compared unless the failure mode differences are accounted for by determining the actual stress states of the film at the location of failure. This example points out the necessity of microscopic examination to determine the failure mode since testing parameters may have a great effect.

Analyses

Variations in styli and film thickness. The scratch test was used only to compare the adhesion of similar systems. It is evident from a theoretical standpoint that variations in styli and film thickness are both very important variables.

Stylus radius and hardness affect the penetration depth of the stylus into the specimen and thus are important factors in the stress distribution under the stylus. Frictional forces, which play a very important role in adhesion failure, are controlled partially by the stylus material and geometry. The point of maximum yield is often below the surface of the specimen. All other factors the same, the thickness of the film defines whether this point lies in the film or in the substrate. Since the material properties of the film and substrate differ, this is a critical consideration.

Analysis based on normal load criterion. The definition of film adhesive strength based on a critical normal load, W, to cause deadhesion was not very consistent. This was not unexpected, however, since it has already been noted that there are a large number of significant parameters involved, including coefficient of friction, which can even vary along the same scratch. For some sets of data, a critical normal load could be defined but since this was not the case for even a majority of the data, the correlation was probably due to the dependence of other factors on the normal load. For example, an increase in the normal load also increased the film and substrate deformations, the radial and shear stresses under the stylus, the mean pressure, the contact area of the stylus, and usually the tangential force.

Analysis assuming full plasticity. Benjamin and Weaver (2) based their analysis of the scratch test on the assumption of full plasticity under the stylus. The shear stress at the lip of the indentation under a load W was defined as

$$F = \{a/(r^2-a^2)^{1/2}\} P,$$

where P is the indentation hardness of the substrate, r is the stylus radius, and a is the contact radius, defined, at full plasticity, as

$$a = (Wg/\pi P)^{1/2}.$$

The shear stresses generated from these equations were also often inconsistent with the loss of film material as defined by light transmission in a microscope. This shear stress increased with the normal load as is predicted from the dependence of the shear force on the normal load. Table 1 shows the shear stresses generated from data for scratches on one of the zirconium/sapphire systems. Although higher shear stresses were more likely to result in film loss, there was no clearly defined critical shear stress above which the film was stripped.

The normal force shown in the tables is the effective normal force applied to the surface after the moment caused by the tangential force is accounted for. This moment occurs because the tangential force is not in a horizontal line with the center of rotation of the scratch tester lever arm and, because of the direction of motion, it serves to lessen the applied normal force on the surface.

Table 2 shows the good correlation between shear stress and film de-adhesion for a chromium/sapphire specimen. In contrast, the only shear stress that did not result in nickel film de-adhesion from sapphire was an intermediate value (See Table 3). This latter may have been due to insufficient data to generate a statistically accurate result.

Table 1. Shear Stresses Calculated Using the Plastic Model Analysis for Scratches on Zirconium/Sapphire.

Normal Force (Newtons)	Tangential Force (Newtons)	Shear Stress (GPa)	Coefficient of Friction	Film De-adhesion
0.0938	0.0128	0.1378	0.136	Yes
0.0948	0.0098	0.1385	0.104	No
0.1410	0.0181	0.1689	0.129	Yes
0.1426	0.0132	0.1699	0.093	Yes
0.1438	0.0098	0.1706	0.068	No
0.1849	0.0332	0.1935	0.179	Yes
0.1906	0.0164	0.1964	0.086	Yes
0.1909	0.0157	0.1966	0.082	Yes
0.2785	0.0464	0.2374	0.167	Yes
0.2844	0.0290	0.2400	0.102	Yes
0.2853	0.0265	0.2403	0.093	Yes
0.2856	0.0255	0.2405	0.089	Yes
0.3717	0.0607	0.2743	0.163	Yes
0.3777	0.0432	0.2765	0.114	Yes
0.3797	0.0373	0.2773	0.098	Yes
0.4664	0.0708	0.3073	0.152	Yes
0.4667	0.0699	0.3074	0.150	Yes
0.4718	0.0549	0.3091	0.116	Yes
0.9126	0.2009	0.4299	0.220	Yes
0.9209	0.1766	0.4318	0.192	Yes

Table 2. Shear Stresses Calculated Using the Plastic Model Analysis for Scratches on Chromium/Sapphire.

Normal Force (Newtons)	Tangential Force (Newtons)	Shear Stress (GPa)	Coefficient of Friction	Film De-adhesion
0.0962	0.0057	0.1395	0.059	No
0.1400	0.0210	0.1683	0.150	No
0.1876	0.0251	0.1949	0.134	No
0.1904	0.0172	0.1963	0.090	No
0.1962	0.0000	0.1993	0.000	No
0.2828	0.0337	0.2393	0.119	No
0.2830	0.0332	0.2394	0.117	No
0.4669	0.0695	0.3074	0.149	No
0.4760	0.0426	0.3104	0.089	No
0.4769	0.0400	0.3107	0.084	No
0.4805	0.0293	0.3119	0.061	No
0.9334	0.1399	0.4347	0.150	No
0.9452	0.1052	0.4375	0.111	No
0.9528	0.0829	0.4392	0.087	No
0.9583	0.0666	0.4405	0.070	No
1.4051	0.1951	0.5334	0.139	No
1.8622	0.2931	0.6141	0.157	Yes
2.3540	0.2893	0.6905	0.123	Yes

Table 3. Shear Stresses Calculated Using the Plastic Model Analysis for Scratches on Nickel/Sapphire.

Normal Force (Newtons)	Tangential Force (Newtons)	Shear Stress (GPa)	Coefficient of Friction	Film De-adhesion
0.9376	0.1274	0.4357	0.136	Yes
1.3840	0.2570	0.5294	0.186	Yes
1.3874	0.2470	0.5301	0.178	Yes
1.3988	0.2135	0.5322	0.153	No
1.8653	0.2839	0.6147	0.152	Yes
1.8660	0.2818	0.6148	0.151	Yes

Another possible explanation may lie in the difference in the deformation modes, as already discussed: the nickel/sapphire systems exhibited ductile extrusion of the film along the scratch path while the chromium films showed no evidence of extrusion. Data taken for nickel/sapphire systems, then, would most likely be very dependent on the mechanical properties of the film and the friction between the film and the stylus and would not lend itself to description by an equation neglecting these factors.

Data from scratches made with a steel stylus on aluminum/glass systems are shown in Table 4. The shear stress in this case correlated well with loss of adhesion. The theoretical and experimental values of the radius of the circle of contact, a, are plotted as a function of normal force in Figure 28. The experimental values were an order of magnitude larger than the theoretical values; this may be due to the failure of the theory to account for the elastic deformation of the system (2).

Analysis assuming elastic conditions. Laugier (7) assumed that adhesive failure of the film can occur under elastic conditions ahead of the stylus. The radial compressive stress ahead of the stylus is given by

$$\sigma = (Wg/2\pi a^2)\ \{(4 + \nu_1)(3\pi f/8) - (1 - 2\nu_1)\},$$

and the shear stress is approximated by

$$\tau \approx \sigma(a/r).$$

This analysis is examined more thoroughly in the Literature Review.

Table 4. Shear Stresses Calculated Using the Plastic Model Analysis for Scratches on Aluminum/Glass.

Normal Force (Newtons)	Tangential Force (Newtons)	Contact Radius (mm)	Shear Stress (GPa)	Coefficient of Friction	Film De-adhesion
0.0013	0.0004	0.0002	0.0023	0.293	No
0.0015	0.0000	0.0002	0.0024	0.000	No
0.0025	0.0013	0.0003	0.0031	0.508	Yes
0.0029	0.0002	0.0003	0.0033	0.068	No
0.0029	0.0000	0.0003	0.0034	0.000	No
0.0035	0.0026	0.0004	0.0037	0.719	Yes
0.0040	0.0013	0.0004	0.0039	0.320	Yes
0.0044	0.0000	0.0004	0.0041	0.000	Yes
0.0044	0.0000	0.0004	0.0041	0.000	Yes
0.0044	0.0000	0.0004	0.0041	0.000	Yes
0.0085	0.0038	0.0006	0.0058	0.450	Yes
0.0085	0.0038	0.0006	0.0058	0.450	Yes
0.0087	0.0032	0.0006	0.0058	0.372	Yes
0.0088	0.0028	0.0006	0.0059	0.322	Yes
0.0092	0.0017	0.0006	0.0060	0.180	Yes
0.0094	0.0011	0.0006	0.0061	0.114	Yes
0.0095	0.0010	0.0006	0.0061	0.104	Yes
0.0175	0.0062	0.0008	0.0083	0.353	Yes
0.0180	0.0048	0.0009	0.0084	0.267	Yes
0.0180	0.0048	0.0009	0.0084	0.267	Yes
0.0180	0.0048	0.0009	0.0084	0.267	Yes
0.0183	0.0038	0.0009	0.0085	0.209	Yes
0.0183	0.0038	0.0009	0.0085	0.209	Yes
0.0184	0.0037	0.0009	0.0085	0.203	Yes
0.0441	0.0144	0.0013	0.0131	0.327	Yes
0.0450	0.0120	0.0014	0.0132	0.266	Yes
0.0451	0.0116	0.0014	0.0133	0.257	Yes

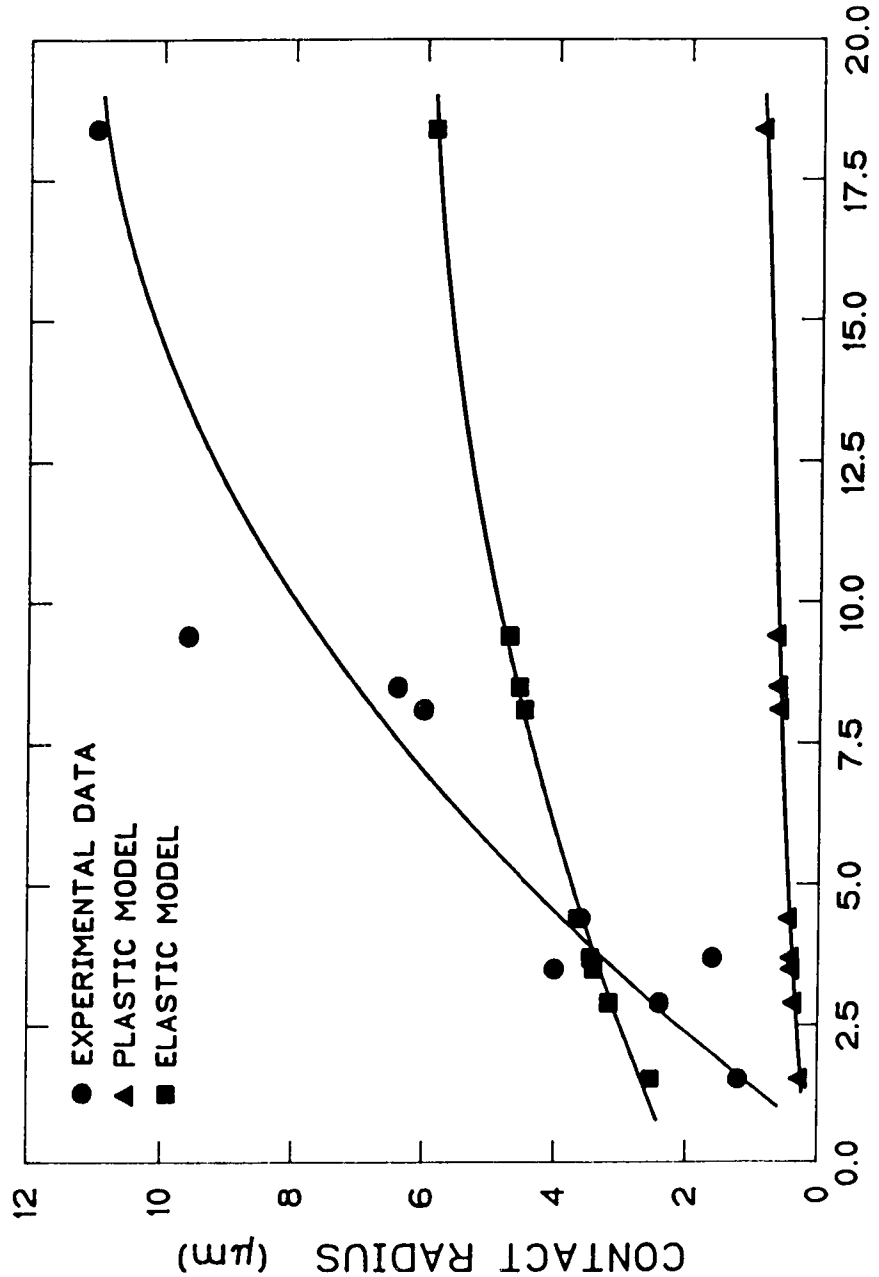


Figure 28. Theoretical and experimental values of the radius of the circle of contact for scratches on aluminum/glass specimens.

The equations of Laugier were used to generate values for the coefficients of friction, radial compressive stresses, shear stresses, and mean pressures for several systems. In each case, the elastic moduli were estimated at bulk substrate material values and Poisson's ratio was taken as 0.3 for all materials. Errors resulting from not using a composite modulus occurred consistently such that the effect was merely to adjust the numbers by a linear factor. Table 5 shows the values of the shear and radial stresses calculated for one set of zirconium/sapphire data. This specimen was chosen because the modulus of zirconium (94.5 GPa) varies by the largest amount from that of its substrate (410 GPa) for the four systems investigated. In some instances, the coefficient of friction was low enough to result in a tensile radial stress and this is denoted by a negative sign in the tables.

Data for the aluminum/glass and the zirconium/sapphire systems show no correlation between the calculated stress values and film de-adhesion. Even some of the tensile stresses generated, which theoretically should not result in film loss, did cause film de-adhesion. This may be due to an inaccurate estimate of Poisson's ratio which could result in this sign change. Figure 28 also shows the radii of the circles of contact for some the scratches made on aluminum/glass specimens and analyzed by this model. For the most part, the theoretical values are less than the experimental values: this is probably because the theory does not account for any plastic deformation, even during the passage of the stylus.

Table 5. Shear Stresses Calculated Using the Elastic Model Analysis for Scratches on Zirconium/Sapphire Comparing the Results Obtained for Different Values of Young's Modulus, E.

Normal Force (Newtons)	Tangential Force (Newtons)	Shear Stress (MPa) Using E of Al_2O_3	Shear Stress (MPa) Using E of Zr	Ratio of Shear Stresses
0.0938	0.0128	6.11	4.07	1.5
0.0948	0.0098	2.65	1.77	1.5
0.1410	0.0181	6.99	4.67	1.5
0.1426	0.0132	1.97	1.31	1.5
0.1438	0.0098	-1.53	-1.02	1.5
0.1849	0.0332	16.9	11.3	1.5
0.1906	0.0164	1.20	0.80	1.5
0.1909	0.0157	0.56	0.38	1.5
0.2785	0.0464	19.4	12.9	1.5
0.2844	0.0290	5.19	3.46	1.5
0.2853	0.0265	3.12	2.08	1.5
0.2856	0.0255	2.33	1.55	1.5
0.3717	0.0607	22.6	15.1	1.5
0.3777	0.0432	9.57	6.39	1.5
0.3797	0.0373	5.23	3.49	1.5
0.4664	0.0708	22.7	15.2	1.5
0.4667	0.0699	22.1	14.8	1.5
0.4718	0.0549	11.8	7.86	1.5
0.9126	0.2009	68.9	46.0	1.5
0.9209	0.1766	55.4	36.9	1.5

As when analyzed by the technique of Benjamin and Weaver, loss of adhesion of chromium from sapphire correlated well with maximum compressive radial stresses, maximum shear stresses, and maximum mean pressures (See Table 6), but these values for the nickel/sapphire systems were intermediate for the only scratch not resulting in film loss (See Table 7). This is probably due to the different deformation modes.

The Pull Test

In theory, the pull test is the most straightforward of the techniques discussed. In practice, however, it is not so easily used. Most of the films used in this research were more adherent to their substrates than the epoxy of the bonding studs was to the film surface or the pin head. Another problem was that the fracture often happened in a complex manner involving several of the interfaces and layers between the pin, epoxy, film, and substrate. Since it was not always known where failure occurred first, it was difficult to determine what the maximum stress reading of the pull tester was actually measuring.

The epoxy pre-coated on the pull test pin was examined under a microscope before curing and found to be continuous but with a few thin spots scattered over the surface. It is hoped that the epoxy became more evenly distributed during curing. The surfaces of the pins were very rough: arithmetic average surface roughnesses were approximately 3 μm. This roughness increased the surface area to which the epoxy could bond and promoted mechanical locking. The ultimate yield

Table 6. Radial and Shear Stresses Calculated Using the Elastic Model Analysis for Scratches on Chromium/Sapphire.

Normal Force (Newtons)	Tangential Force (Newtons)	Radial Stress (GPa)	Shear Stress (MPa)	Film De-adhesion
0.4805	0.0293	-0.187	-5.70	No
0.9584	0.0665	-0.126	-4.82	No
0.0962	0.0057	-0.121	-2.15	No
0.4769	0.0400	0.052	1.57	No
0.1904	0.0172	0.086	1.93	No
0.4760	0.0426	0.109	3.31	No
0.9528	0.0829	0.106	4.04	No
0.2830	0.0332	0.335	8.54	No
0.2828	0.0337	0.354	9.02	No
0.1876	0.0251	0.419	9.33	No
0.1400	0.0210	0.492	9.93	No
0.9452	0.1052	0.423	16.1	No
0.4669	0.0695	0.723	21.8	No
0.9334	0.1399	0.925	35.1	No
1.4051	0.1951	0.895	39.0	No
2.3540	0.2893	0.780	40.3	Yes
1.8622	0.2931	1.290	61.6	Yes

Table 7. Radial and Shear Stresses Calculated Using the Elastic Model Analysis for Scratches on Nickel/Sapphire.

Normal Force (Newtons)	Tangential Force (Newtons)	Radial Stress (GPa)	Shear Stress (MPa)	Film De-adhesion
0.9376	0.1274	0.74	28.3	Yes
1.3988	0.2135	1.10	47.8	No
1.8660	0.2818	1.18	56.7	Yes
1.8653	0.2839	1.20	57.6	Yes
1.3874	0.2470	1.47	63.9	Yes
1.3840	0.2570	1.59	68.8	Yes

strength of the epoxy was specified as 62 to 69 MPa and this was usually achieved before the epoxy or either of its interfaces failed.

Stresses developed in the specimens during film growth and cooling can greatly affect the results of the pull test. For one set of chromium films evaporated onto glass substrates, the substrates were under sufficient compression under the film that the test pin removed, not the film from the substrate, but a hemispherical section of glass of approximately the same diameter as the test pin. Test pins epoxied directly to the glass, where no film was present to put the substrate in compression, did not have this effect, even to much greater loads.

Two techniques were used to introduce reproducible flaws into the film in an attempt to lower the apparent adhesion of the film to within the range of the pull tester.

In the first method, a Vickers hardness indent was made on the film surface. The cracks propagating from the corners of the pyramidal indent served as the flaws that might lead to film de-adhesion. Unfortunately, this proved not to be the case: the adhesion of the films remained beyond the range of the tester, probably because the cracks were too small. Even if this had worked, it would be very difficult to analyze an apparent adhesion increase due to ion beam mixing because it is not known precisely how the mixing affects the parameters involved. It is known qualitatively from other researchers that ion beam mixing increases surface hardness (54,55,56) and inhibits crack propagation (59). These variations between mixed and unmixed films would mean that cracks produced by a standard indent load on unmixed

material could not be exactly reproduced on a mixed system and the flaw itself would become a variable in the analysis.

In the second method, a thin layer of gold was sputter deposited onto a small portion of the substrate. The test film was then deposited through a mask such that a portion of this new film overlapped the gold layer. Since the gold was non-adherent (experimentally) to the sapphire and glass substrates, this served as a release layer for the test film and the resulting failure was treated from a fracture mechanics point of view. The mild shadowing effect of the mask used during gold deposition caused the edge of the gold layer under the test film to be tapered and thus this was treated as a reproducible crack and the analysis made using the concept of fracture toughness as indicated by the stress intensity factor, K. For the Mode I crack opening mode, K_I is given in ASTM Special Technical Publication 410 (60) as

$$K_I = 1.1 \sigma \sqrt{\pi a} ,$$

where $\underline{a}$ is the crack length and σ is the normal stress.

Since the point of the analysis was not to determine a material property but to find some means of comparison of the fracture strength for similar but flawed systems, it was not significant that the specimens used in this research did not meet the specimen size requirements given for fracture toughness testing. All specimens used for comparison were of almost identical shape and size.

By using K_I, which incorporates the geometry of the crack, errors in pin placement were not as critical since they were accounted for by careful measurement of the crack length.

This latter method of a gold release layer was used to investigate the adhesion of 500 nm zirconium films on sapphire substrates. The gold layer was approximately 20 nm thick. For comparison, some pull tests were performed on areas of the test film that did not overlap the release layer. None of the pulls performed without a release layer resulted in any film loss. The other tests resulted in varying amounts of film loss over a wide range of applied stresses (See Table 8). Note that the specimen with the largest percentage of test film removed had an intermediate value of K_I.

It was assumed that the epoxy failed first in the cases where both the film/substrate interface and one of the epoxy interfaces failed and the stresses were recalculated for the actual area supporting the load. Such calculated stresses were much higher than the tensile strength of the epoxy. This was deemed unreasonable and it was thus assumed that the zirconium/sapphire interface failed first at some stress less than the final maximum reading at which stress the remaining epoxy failed. Calculation of the stresses based on this assumption gave stresses on the remaining intact system that were approximately equal to the tensile strength of the epoxy. This latter, then, was a reasonable assumption. Since the stress to cause failure of at least part of the test film occurred at a smaller stress than the maximum shown in Table 8, it can be concluded that the stress intensity factors in Table 8 represent an upper limit of those required to cause film de-adhesion.

The gold layer does have an effect on the stress intensity. Table 8 reveals the adhesive strength of the film to the substrate to be

Table 8. Pull Test Results for Specimens with Gold Release Layer.[a]

Specimen Number	Gold Release Layer	Stress at Failure (MPa)	Maximum Crack Length (mm)	Stress Intensity Factor (MPa$\sqrt{m}$)	Test Film Removed (Percent)
477 c	No	64.74	---	---	0
477 d	No	59.57	---	---	0
478 b	No	69.98	---	---	0
480 d	No	56.75	---	---	0
478 a	Yes	5.45	0.396	0.212	26
479 c	Yes	35.10	0.770	1.899	20
480 a	Yes	38.61	1.389	2.806	13
480 b	Yes	25.65	0.472	1.086	65

[a]Different identification letters refer to separate tests on the same specimen. "Test film removed" refers to the test area not including that over the release layer.

greater than 55 MPa (the strength of the epoxy) if no release layer is present. If the effect of the layer were solely to reduce the effective area supporting the applied load, thus increasing the stress on the system, recalculation of the stresses based on the area under the pin but not over the gold layer should reveal maximum stresses of about the same order of magnitude as when no release layer was utilized. Table 9 shows this not to be the case: the stresses recalculated for the specimens omitting the pin area over the gold material were in general much less than the strength of the epoxy. Failure would not have occurred at these low stresses if the release layer did not have an effect on the stress intensity.

Some reasons that the crack resulting from the gold layer did not propagate further between the test film and substrate include: (a) the gold may not have been completely continuous at a thickness of 20 nm; (b) the crack tip caused by the edge of the layer may not have been sharp enough; and (c) the zirconium film may not have been continuous over the edge of the gold. Also, gold on sapphire tends to agglomerate during heating and this may have occurred during the test film deposition or during the epoxy cure cycle. More extensive crack propagation might be obtained after the investigation of these factors.

Effects of Ion Beam Mixing

Adhesion to Sapphire Substrates

Scratch adhesion. The scratch test was utilized to investigate the effect of ion beam mixing on film adhesion for chromium, nickel, and zirconium films on sapphire substrates.

Table 9. Stresses Recalculated Assuming Reduced Area Under the Pin by Omitting Area Over the Gold Release Layer.

Specimen Number	Stress at Failure Recalculated Omitting Pin Area Over Gold Layer (MPa)
478 a	5.79
479 c	38.68
480 a	71.29
480 b	38.47

The as-deposited thicknesses of the zirconium, chromium, and nickel films were 0.18, 0.17, and 0.20 μm, respectively. It was found from the E-DEP-1 code (58) that the average projected ranges (the depth at which most of the ions come to rest) of Fe^+ ions into these materials were 0.47, 0.36, and 0.31 μm, respectively. Since the shape of the concentration of iron ions versus depth curve is generally gaussian, only a relatively few iron ions came to rest in the film. The computer code "Profile" (61), which calculates the distributions of ions implanted into surfaces, revealed that the maximum concentration of the iron ions, which occurs at the interface and diminishes quickly away from the interface, was less than 6.5 atomic percent for the nickel film and was even less for the other films. Thus, it was reasonable to assume that the structural and alloying effects were minimal. The cause of the "ion beam mixing" was instead the energy transferred and the defects created near the interface due to the collisions associated with the passage of the ion.

For some of the chromium/sapphire and zirconium/sapphire specimens, the scratch test data revealed critical values of the normal load, plastic shear stress, and elastic shear stress necessary to cause de-adhesion, while the data for other specimens was very inconsistent and no critical values were discernable. This difference may be due to some unrecognizable difference in the specimens themselves or to some uncontrollable testing conditions, such a air humidity or stylus damage.

For those specimens exhibiting critical values for de-adhesion, ion beam mixing greatly improved the adhesion of the chromium films.

Although there was a large amount of scatter in the data, normal forces as low as 0.20 N resulted in film stripping in the unmodified regions while none of the scratches in the modified region resulted in a loss of adhesion, even for normal forces as high as 3.92 N. Critical shear stresses calculated from the equations of Benjamin and Weaver which assumed fully plastic conditions showed a marked improvement of 350 percent for one of the specimens (See Table 10). Analysis of data for the same specimen using Laugier's elastic equations also revealed an increase in the critical shear stress of over 300 percent (See Table 11).

No increase in the adhesion of nickel films to sapphire substrates was evident among the wide scatter of the data obtained by each of the analysis methods. This scatter may be due to the extrusion of nickel films under the stylus, as previously discussed.

Two sets of data were taken and analyzed for the zirconium/sapphire systems. For the first set, normal forces as low as 0.094 N and shear stresses calculated from the plastic model as low as 0.13 GPa resulted in film de-adhesion in the unmixed region while normal forces as high as 0.94 N and shear stresses as high as 0.44 GPa failed to cause de-adhesion in the ion beam mixed regions. These numbers represent an increase of 900 and 230 percent, respectively, due to the mixing. However, analysis assuming elastic conditions for this set showed no correlation between the radial and shear stresses and film de-adhesion. As already discussed, these films were subject to tensile failure behind the moving stylus so the elastic theory concerning failure ahead of the stylus would not provide an adequate description.

Table 10. Comparison of Critical Shear Stresses Calculated Using the Plastic Model Analysis for Scratches on Chromium/Sapphire.

Normal Force (Newtons)	Tangential Force (Newtons)	Shear Stress (GPa)	Film De-adhesion	Ion Beam Mixed
0.1875	0.0254	0.1949	Yes	No
0.9464	0.1016	0.4378	Yes	No
0.9464	0.1016	0.4378	Yes	No
0.9464	0.1016	0.4378	Yes	No
0.9474	0.0988	0.4380	Yes	No
2.3492	0.3034	0.6898	Yes	No
2.3554	0.2851	0.6908	Yes	No
2.3564	0.2822	0.6909	Yes	No
2.3564	0.2822	0.6909	Yes	No
2.3799	0.2133	0.6943	Yes	No
2.3799	0.2133	0.6943	Yes	No
3.7817	0.4178	0.8818	No	Yes
3.7817	0.4178	0.8818	No	Yes

Table 11. Comparison of Critical Shear Stresses Calculated Using the Elastic Model Analysis for Scratches on Chromium/Sapphire.

Normal Force (Newtons)	Tangential Force (Newtons)	Shear Stress (MPa)	Film De-adhesion	Ion Beam Mixed
0.1875	0.0254	9.60	Yes	No
2.3799	0.2133	9.85	Yes	No
2.3799	0.2133	9.85	Yes	No
0.9474	0.0988	12.7	Yes	No
0.9464	0.1016	14.2	Yes	No
0.9464	0.1016	14.2	Yes	No
0.9464	0.1016	14.2	Yes	No
2.3564	0.2822	37.5	Yes	No
2.3564	0.2822	37.5	Yes	No
2.3554	0.2851	38.6	Yes	No
2.3492	0.3034	46.0	Yes	No
3.7817	0.4178	39.7	No	Yes
3.7817	0.4178	39.7	No	Yes

For the second set of zirconium/sapphire data, the highest values of the normal load and the plastic model shear stress resulted in film de-adhesion but there was no increase in these critical values with ion beam mixing. No critical stresses could be determined for this set using the elastic analysis for either the mixed or unmixed regions.

Tensile adhesion. The pull test was also used to investigate the adhesion of the zirconium films. Even in the unmixed condition, the adherence of the test films was beyond the range of the tester so a gold release layer was used to initiate failure. Unfortunately, this was sometimes still insufficient to cause de-adhesion. Most of the failures that did occur involved several of the interfaces in the system and thus the analysis was not straightforward. Another problem encountered was that ion beam mixing also greatly increases the adhesion of gold to sapphire so additional care was needed to ensure correct placement of the specimen masks such that no gold was mixed.

Gold was chosen for the release layer material because it does not "wet" sapphire. Because of its non-wetting characteristics, and thus non-adherence, the gold film and the superimposed test film were often removed during sample preparation and handling. As a result, data for the ion beam mixed case were gathered for only one ion beam condition. In each of the pull tests in the ion beam mixed region, the only part of the zirconium film removed was that directly over the gold layer: the crack caused by the presence of the gold did not propagate between the mixed film and the substrate. The crack length for the test performed on the same specimen in the unmixed region was intermediate to the crack

lengths utilized in the mixed region (See Table 12). The average maximum stress at failure and the average stress intensity factor for the mixed region were greater than the upper limits of these for the unmixed region (From Table 8, Page 80) by 40 and 30 percent, respectively. This indicated significant adhesion enhancement by ion beam mixing since both regions had similar flaws but the mixed region withstood a greater stress and a greater stress intensity factor with no zirconium removal.

Adhesion to Silicon Carbide and Silicon Nitride Substrates

The effect on thin film adhesion of ion beam mixing was also investigated for four material systems having silicon nitride or silicon carbide as substrates:

1. 30 nm aluminum on silicon nitride;
2. 30 nm aluminum on silicon carbide;
3. 30 nm zirconium on silicon carbide;
4. 15 or 30 nm zirconium on silicon nitride.

The pull test was utilized to test the adhesion of these films to their substrates since the opaqueness of the substrate meant that light transmission through the film could not be used to judge de-adhesion by scratching. Optical and scanning electron microscopy, surface profilometry, and energy dispersive x-ray spectroscopy were all used to determine which interfaces and layers failed.

Scanning electron microscopy revealed the films to be porous and somewhat discontinuous due to a rough, polycrystalline substrate surface (See Figure 29). An additional layer of the original film material was evaporated onto the surface in order to have a more continuous surface

Table 12. Pull Test Results for Ion Beam Mixed Specimens.[a]

Specimen Number	Stress at Failure (MPa)	Maximum Crack Length (mm)	Stress Intensity Factor (MPa$\sqrt{m}$)	Test Film Removed (Percent)
479 a (mixed)	37.03	0.942	2.22	0
479 b (mixed)	60.68	0.546	2.76	0
479 c	35.10	0.770	1.90	20

[a]Different identification letters refer to separate tests on the same specimen. "Test film removed" refers to the test area not including that over the gold release layer.

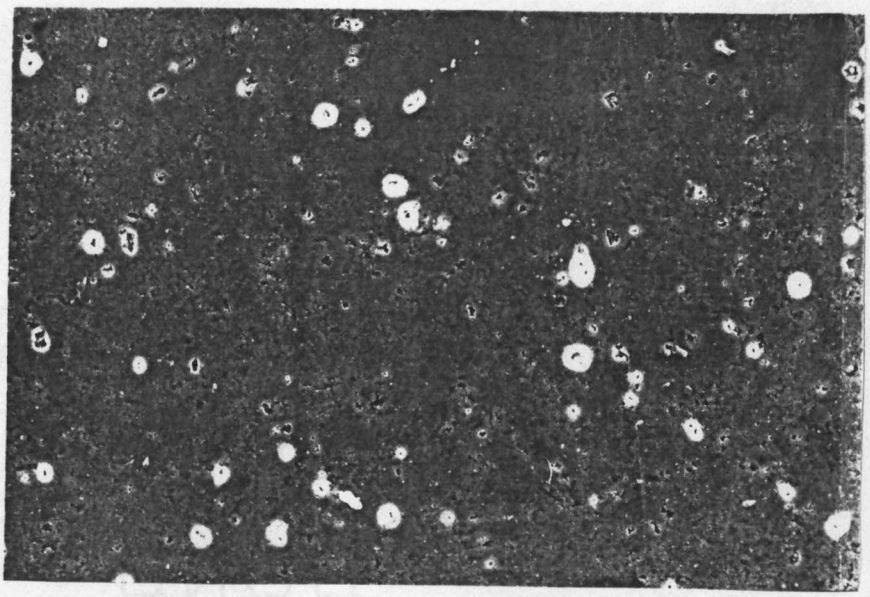


Figure 29. Original 30 nm zirconium film on silicon carbide. The bright spots are electron discharges from the substrate, revealing the pores in the film. Scanning electron micrograph, 300X.

against which to epoxy the pull test pins. This layer was evaporated after the ion beam mixing was complete because the ion energies utilized in this experiment were insufficient to penetrate the thicker films.

In preparation for the second deposition, both the aluminum coated specimens were cleaned in Micro laboratory cleaning solution. The parting agent of this solution removed some of the original aluminum films from their substrates. Based on visual inspection, a very thin layer may have remained, particularly in the ion beam mixed regions, but this could not be quantified. As a result of this experience, the cleaning procedure was discontinued for all specimens already bearing a film. The additional aluminum layer was deposited on the substrate as planned.

Aluminum film on silicon nitride. The test conditions examined for the aluminum on silicon nitride were:

1. 200 nm aluminum, as deposited (no underlying layer);
2. 200 nm aluminum plus an underlying layer of unknown thickness, as deposited;
3. 200 nm aluminum plus an underlying layer of unknown thickness, ion beam mixed to a dose of 0.5×10^{16} ions/cm^2 at an energy of 200 keV.

In the pull test, all failures in all three of the regions occurred at zero measurable force. Surface profilometry and energy dispersive x-ray spectroscopy confirmed that the aluminum film was completely removed under the test pins. Based on this data, it was concluded that the

adhesion of the aluminum to the silicon nitride was very poor and the ion beam mixing had no measurable effect.

This experiment gave insight into some aspects of the pull test. Several of the pins broke from the specimen, removing the film from the substrate, during the manual procedure of inserting the shank of the pin into the testing machine. From a practical viewpoint, it is very difficult to insert the pin without touching it to some portion of the unit and thus exerting some unknown forces and moments. Also, the grips of the tester must be tightened onto the shank below the platen and this, too, can exert a moment on the film as the specimen is drawn down into the platen and aligned. Although these forces may be sufficient to remove the film from the substrate, as in this case, they cannot be quantified. Thus the pull test has a lower limit as well as the previously discussed upper limit.

Aluminum film on silicon carbide. Four types of regions were examined for the aluminum film on the silicon carbide substrate:

1. 200 nm aluminum, as deposited (no underlying layer);
2. 200 nm aluminum plus an underlying layer of unknown thickness, as deposited;
3. 200 nm aluminum plus an underlying layer of unknown thickness, ion beam mixed to a dose of 0.5×10^{16} ions/cm^2 at an energy of 200 keV;
4. 200 nm aluminum plus an underlying layer of unknown thickness, ion beam mixed to a dose of 2.0×10^{16} ions/cm^2 at an energy of 200 keV.

The pull test results are summarized in Table 13. These data reveal a significant increase in adhesion as a result of ion beam mixing, and the strength of the bond increased with ion dose. The presence of the underlying layer made no difference for the unmixed films. Energy dispersive x-ray spectroscopy measurements showed clearly that the failure occurred at the aluminum/silicon carbide interface and not within the aluminum film itself.

As already noted, the original ion beam mixed film may have been removed during the cleaning procedure. If so, the adhesion increase of the additional film to the substrate may be due to a change in the wetability or surface energy of the substrate as a result of the ion bombardment. This is consistent with the work of Baglin and Clark (53) who have reported that ion irradiation lowers the interfacial energy and thus enhances adhesion.

If the film was only partially removed, the portions remaining would be those with the best adhesion to the substrate. If the adhesion of the second film to the first is good, as it proved to be in this case, the adhesion increase due to the mixing of the first film would be reflected in the results of the pull test.

Zirconium film on silicon carbide. The film adhesion was tested for four film conditions for the zirconium on silicon carbide:

1. 30 plus 500 nm zirconium, as deposited;
2. 30 plus 500 nm zirconium, ion beam mixed to a dose of 0.5×10^{16} ions/cm^2 at an energy of 200 keV;

Table 13. Pull Test Strength of Aluminum Film on Silicon Carbide Substrate.

Region	Dose ($\times 10^{16}$ ions/cm^2)	Average Pull Strength (MPa)
a	0	0
b	0	0
c	0.5	24.82
d	2.0	37.92

3. 30 plus 500 nm zirconium, ion beam mixed to a dose of 2.0×10^{16} ions/cm^2 at an energy of 200 keV;
4. 30 plus 500 nm zirconium, ion beam mixed to a dose of 2.0×10^{16} ions/cm^2 at an energy of 350 keV.

The data gathered from these pull tests is rather difficult to interpret since the failure was of a complex nature involving several of the interfaces between the pin, epoxy, film, and substrate. Judgement of which interface failed was based on inspection of the test site--if epoxy remained on the specimen surface, it was deemed that the pin/epoxy interface failed; if the film was the topmost layer, the epoxy/film interface failed; and if the substrate was exposed, failure occurred at the film/substrate interface.

Assuming that the pin/epoxy interface failed first in the tests where both the film/substrate and the pin/epoxy interfaces experienced failure, the remaining portions of the film/substrate interface then failed at the maximum measured load. Recalculation of the stress based on the measured areas of film removed resulted in stresses ranging up to 1,696 MPa. This is not a likely situation, since the tensile strength of the epoxy, still carrying the load from the tester to the interface, is approximately 69 MPa.

If, however, it is assumed that the film/substrate interface failed locally first at some low load, leaving a epoxy/film/substrate system intact to carry the load, the maximum stresses can be recalculated based on the area of film remaining. These maximum stresses are much closer to the specified maximum epoxy strength and thus this is the more likely

scenario. Very localized failure of the film/substrate interface is also supported by the observation that the areas of film removed from the substrate are generally very small spots rather than continuous regions and the total area of these spots averages only about 15 percent of the total pin contact area (See Figure 30). Since the film/substrate interface is not disrupted in general, but only locally, the adhesion strength can be specified as being greater than the maximum stress reported.

The results for the two zirconium/silicon carbide specimens are shown in Table 14. For the first set, ion beam mixing did not appear to have much effect, although it should be noted that only the region receiving the larger dose at the higher energy exhibited a strength greater than the mean of the given values. For the second set, the larger dosed region exhibited a marked adhesion increase.

As previously mentioned in Chapter III, the specimens undergo a mild thermal cycle in the course of the second film deposition. For one of the zirconium/silicon carbide systems, this cycle produced sufficient thermal stress such that, combined with the internal stresses generated in the film growth, film de-adhesion occurred spontaneously. This de-adhesion, however, was not uniform across the three regions of the specimen represented on this bar and it appeared to be a function of ion dose. Figure 31 shows the specimen surface in areas that have not been ion beam mixed on either end of the mixed segment. The de-adhesion of Figure 31 is shown at higher magnification in Figure 32. Figures 33 and 34 show the surface in regions that have been ion beam mixed to a dose

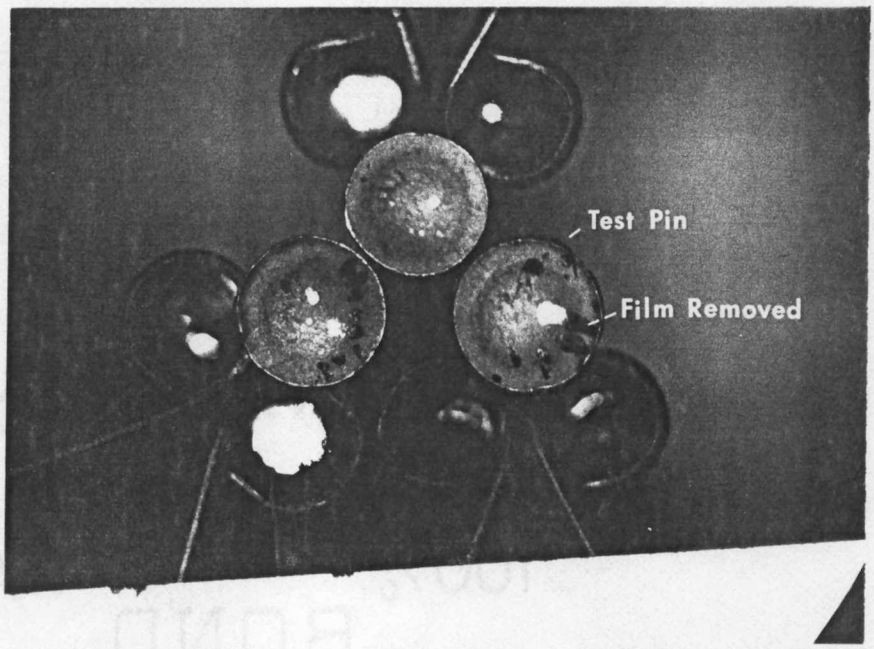


Figure 30. Dark spots of film removed with the test pins. 8X.

Table 14. Pull Test Strength of Zirconium Film on Silicon Carbide Substrate.

Specimen Number and Region	Dose ($\times 10^{16}$ ions/cm^2)	Energy (keV)	Pull Strength in Excess of (MPa)
1 a	0	---	75.22
1 b	0.5	200	68.05
1 c	2.0	200	65.43
1 d	2.0	350	89.64
2 a	0	---	0
2 b	0.5	200	0
2 c	2.0	200	59.09

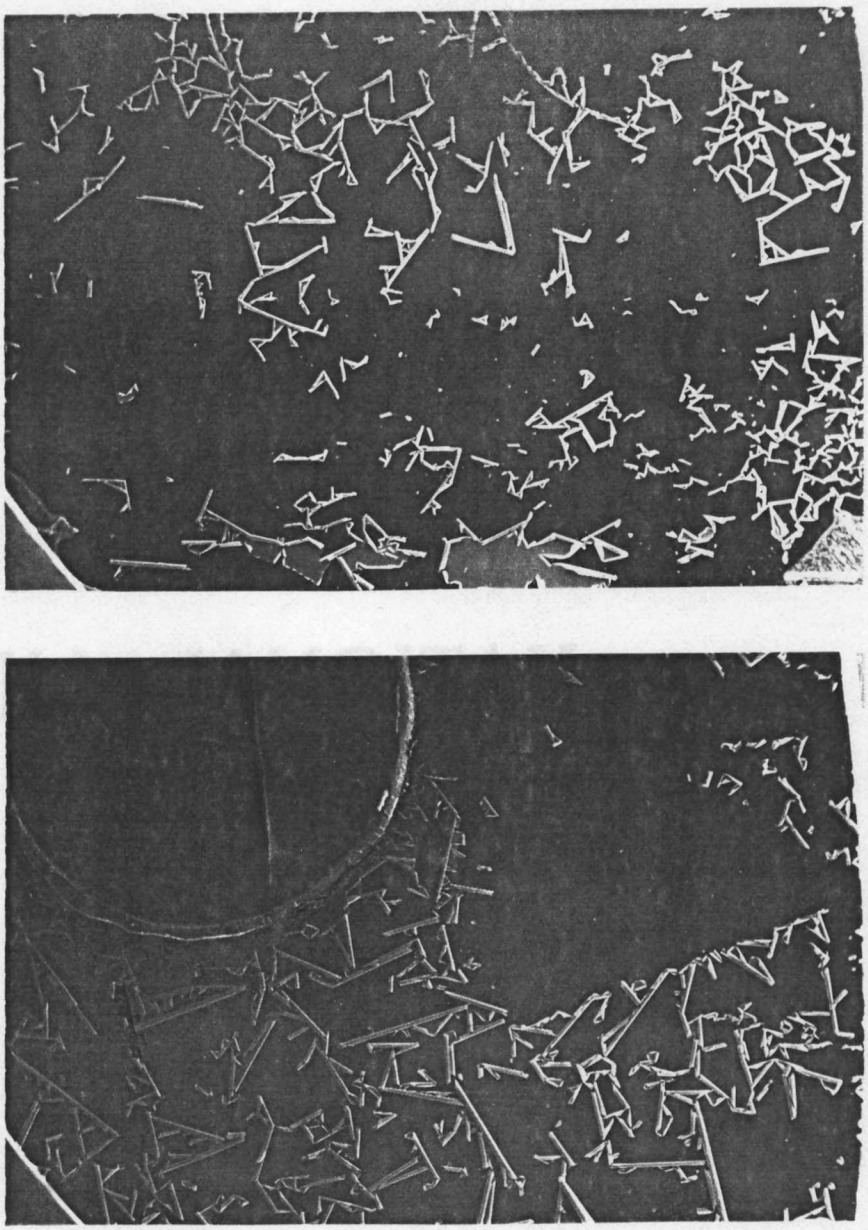


Figure 31. De-adhesion of zirconium film from silicon carbide specimen surface in unmixed regions. Scanning electron micrograph, 20X.

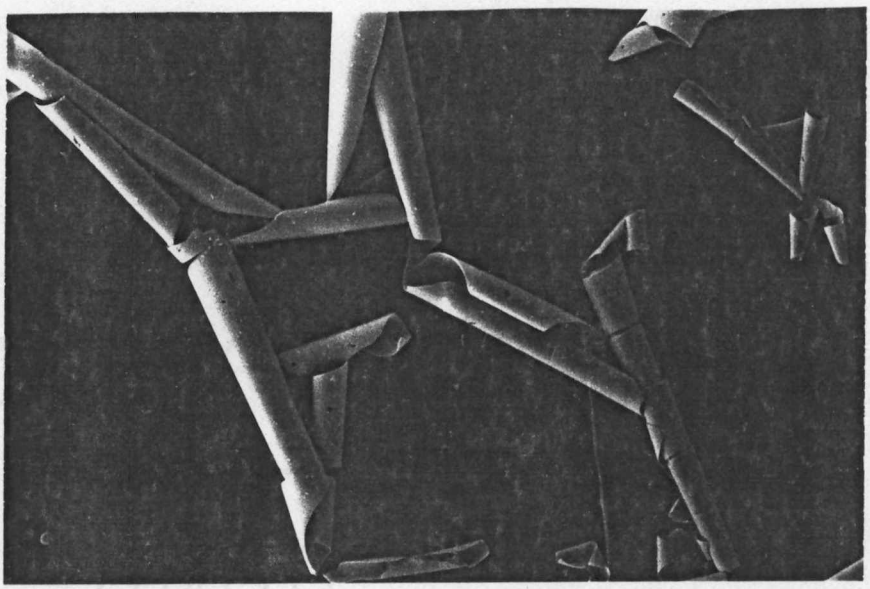


Figure 32. De-adhesion of Figure 31 at higher magnification. Scanning electron micrograph, 250X.

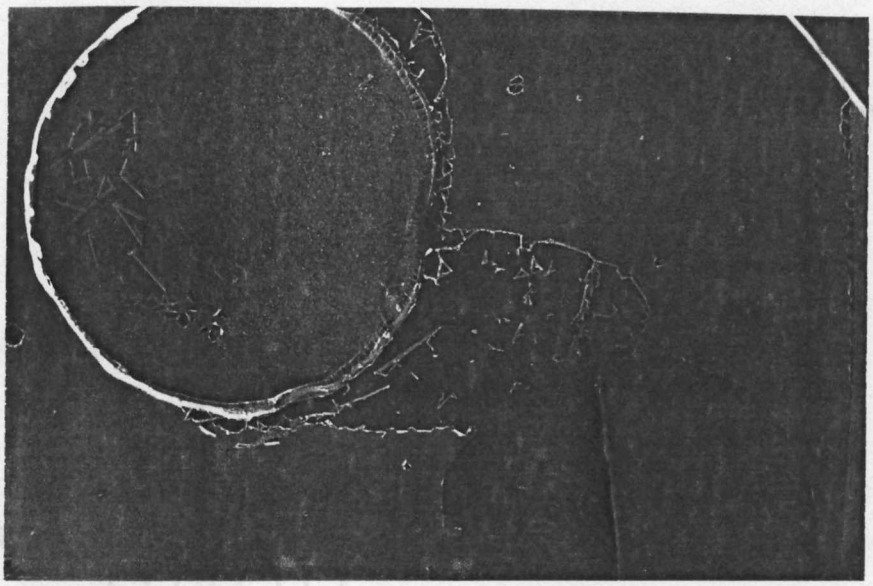


Figure 33. Zirconium on silicon carbide specimen surface, ion beam mixed to a dose of 0.5×10^{16} ions/cm^2. Scanning electron micrograph, 20X.

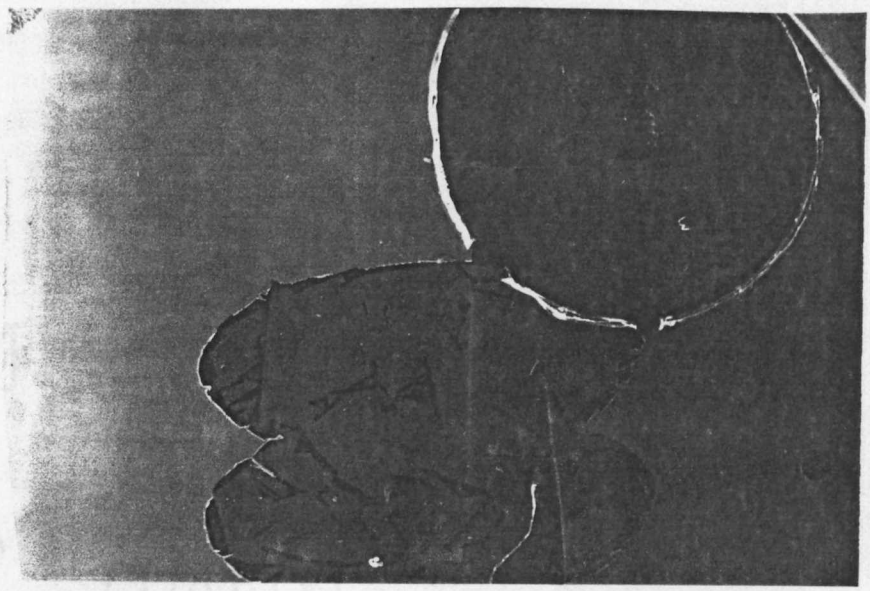


Figure 34. Zirconium on silicon carbide specimen surface, ion beam mixed to a dose of 2.0×10^{16} ions/cm^2. Scanning electron micrograph, 20X.

of 0.5 and 2.0 × 10^{16} ions/cm^2, respectively. In these micrographs, the film material appears as a lighter gray than the substrate. The oval regions are areas damaged during Rutherford backscattering experiments and the circles are the pull test sites.

The interpretation of these pictures is as follows. The adhesion of the additional 500 nm zirconium to the original 30 nm zirconium was very good. However, large tensile stresses were developed in the additional layer during growth and cooling. The same stresses were present throughout the length of the specimens but had a different effect in the various regions due to differences in adhesion of the original layer. In areas that had not been ion beam mixed, the internal stresses were sufficient to cause de-adhesion of the entire 530 nm film. In regions that had been ion beam mixed, the adhesion of the original 30 nm film was generally adequate to prevent the film from de-adhering and curling up, especially at the higher doses. Only very small regions of de-adhesion are visible in the mixed films, and these are fewer in the higher dosed region.

Zirconium film on silicon nitride. The original layer of zirconium was deposited in two different thicknesses, 15 and 30 nm, on the silicon nitride substrates.

For the specimen consisting of an original 15 nm zirconium film, the test parameters were:

1. 500 nm zirconium, as deposited;
2. 515 nm zirconium, as deposited;

3. 515 nm zirconium, ion beam mixed to a dose of 0.5×10^{16} ions/cm^2 at an energy of 200 keV.

Upon testing, only in the ion beam mixed region did failure occur at a non-zero applied load. Assuming, as before, that failure occurred first at the pin/epoxy interface and the remaining film supported the load (i.e. stress recalculated based on area of film removed), the strength of the film/substrate interface was 172 MPa. As noted, this is unrealistic since the tensile strength of the epoxy is only 69 MPa. Assuming the film/substrate interface failed locally first, the adhesive strength of the film to the substrate is in excess of 61.7 MPa. Compared with the zero strength values obtained for the unmixed region, this shows a significant adhesion increase (Table 15).

This specimen also underwent some spontaneous de-adhesion due to the internal stresses generated in growth and cooling. The ion beam mixed film is significantly more continuous than the unmixed region (Figures 35 and 36), indicating better film adhesion to the substrate as a result of the ion beam mixing.

The test parameters for the specimen bearing an original 30 nm zirconium film were:

1. 530 nm zirconium, as deposited;
2. 530 nm zirconium, ion beam mixed to a dose of 0.5×10^{16} ions/cm^2 at an energy of 200 keV;
3. 530 nm zirconium, ion beam mixed to a dose of 2.0×10^{16} ions/cm^2 at an energy of 200 keV;
4. 530 nm zirconium, ion beam mixed to a dose of 2.0×10^{16} ions/cm^2 at an energy of 350 keV.

Table 15. Pull Test Strength of 515 nm Zirconium Film on Silicon Nitride Substrate.

Region	Dose ($\times 10^{16}$ ions/cm^2)	Average Pull Strength in Excess of (MPa)
b	0	0
c	0.5	61.71

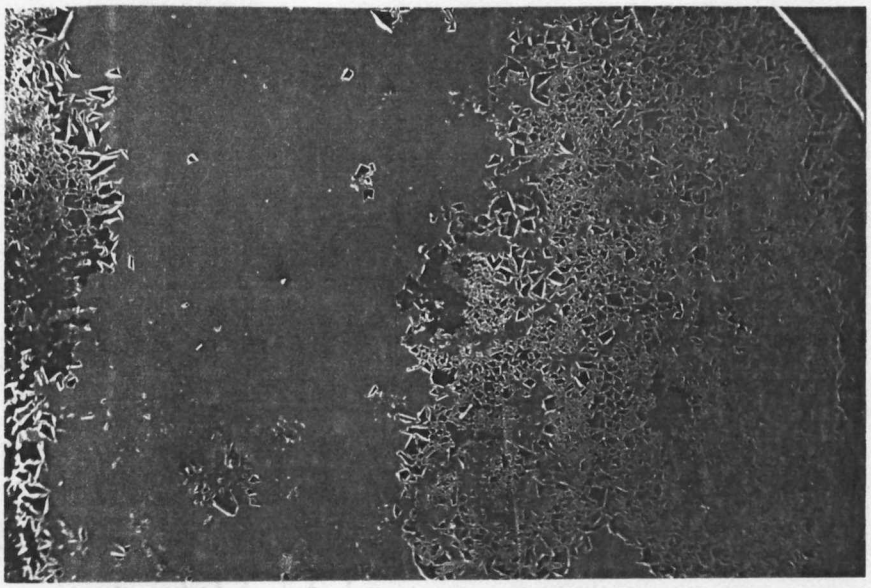


Figure 35. Zirconium (515 nm) on silicon nitride specimen surface in unmixed region. Scanning electron micrograph, 20X.

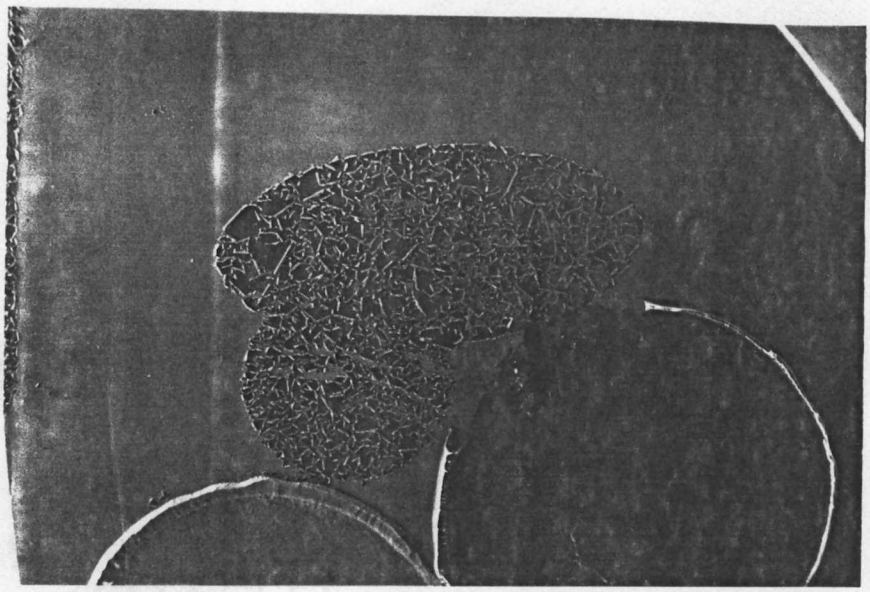


Figure 36. Zirconium (515 nm) on silicon nitride specimen surface in mixed region. Scanning electron micrograph, 20X.

For the 530 nm zirconium film on the silicon nitride substrate, the adhesion values, based on the theory that the film/substrate interface fails locally first since the areas of film removed are very small, ranged from 6.1 to 61 MPa (Table 16). No increase in the adhesion of the film to the substrate could be detected but the strength of the pin/epoxy interface was consistently poor, preventing the detection of a more accurate limits for the adhesion strength.

Table 16. Pull Test Strength of 530 nm Zirconium Film on Silicon Nitride Substrate.

Region	Dose ($\times 10^{16}$ ions/cm^2)	Energy (keV)	Average Pull Strength in Excess of (MPa)
a	0	---	47.13
b	0.5	200	23.72
c	2.0	200	6.07
d	2.0	350	24.75

CHAPTER V

CONCLUSIONS

Each of the testing methods discussed can reveal information about the adhesion of a thin metallic film to a ceramic substrate. This information is different for each of the tests, however, because the loading mechanisms, the stress states induced, and the material responses measured are different. It is essential that these aspects of the tests, as well as the variables on which each depends, be understood and controlled before any significance can be given to the data.

The Scratch Test

Although each of the analyses of the scratch test was based on a great many assumptions and each failed to consistently yield a critical value of some stress which would result in film de-adhesion, these analyses gave insight into the stress state of the system and revealed some of the variables that must be examined, such as hardness and modulus of elasticity. Both the plastic and elastic models correlated well with film de-adhesion for the chromium/sapphire systems which showed no evidence of ductile extrusion but neither correlated well with de-adhesion of the nickel film, which was subject to extrusion. Only the plastic model yielded critical values for the aluminum/glass and zirconium/sapphire systems. It has been shown that the zirconium films often cracked along the lines of maximum tensile stress behind the moving stylus and, since this was not a possibility in the elastic ana-

analysis, it was not unexpected that this latter model failed to describe a critical value for these systems.

While a critical normal load and critical plastic shear stress were usually identifiable for poorly adherent systems such as aluminum to glass, the results of the scratch test on well adherent films can be explained in terms of the relative ductilities of the film materials. For relatively brittle films, such as chromium, critical normal loads, critical plastic shear stresses, and critical elastic shear stresses existed. For ductile materials, such as nickel, none of the analyses methods discussed revealed a critical value for film de-adhesion. Zirconium films have an intermediate ductility and sometimes exhibited the phenomena of critical normal loads and critical plastic shear stresses. Thus the adhesion of brittle metallic films can be described in terms of critical values resulting from the scratch test while ductile films, the scratching of which depends more on the properties of the film than the adhesion, cannot. Table 17 shows the elongations to failure for the bulk materials (62-65), which may be different for the thin films but should maintain the same ranking, and summarizes these conclusions.

The definition of a critical normal load or critical plastic shear stress (which is directly dependent on the normal load) was not always possible, even for brittle films. This implies that the correlation was not due simply to the normal load but rather to some other parameter or combination of factors that was also dependent on the normal load. For some sets of conditions, this latter relationship was straightforward

Table 17. Analysis Methods Useful in the Determination of Critical Values for Film De-adhesion for the Systems Investigated.

System	Elongation in 5.08 cm Gage Length (Percent)	Normal Load Analysis	Plastic Shear Stress Analysis	Elastic Shear Stress Analysis
Cr/Al_2O_3	0[a]	Yes	Yes	Yes
Zr/Al_2O_3	19[b]	Yes	Yes	No
Ni/Al_2O_3	50[c]	No	No	No
Al/Glass	65[d]	Yes	Yes	No

[a] Encyclopedia of Engineering Materials and Processes, H. R. Clauser, ed. in chief, Reinhold Publishing Corporation, New York, 1963, p. 149.

[b] Encyclopedia of Engineering Materials and Processes, H. R. Clauser, ed. in chief, Reinhold Publishing Corporation, New York, 1963, p. 768.

[c] Encyclopedia of Engineering Materials and Processes, H. R. Clauser, ed. in chief, Reinhold Publishing Corporation, New York, 1963, p. 440.

[d] Ross, Robert B., p. 4 in Metallic Materials Specification Handbook, Third Edition, E. & F. N. Spon, London, 1980.

enough that the adhesion could be measured by the critical normal load. Thus, while the scratch test can result in the description of a critical load, it is very difficult to get reliable data and many factors must be considered.

The Pull Test

The pull test is a relatively straightforward technique when the tensile adhesion of the film is less than the strength of the epoxy. For some of the specimens examined in this research, where this was not the case, a release layer was utilized to induce a stress intensity factor at the film/substrate interface that caused de-adhesion at a load within the range of the tester. The analysis was analogous to that used in fracture toughness testing using the Mode I crack opening mode. Comparison of film adherence was based on the calculation of the stress intensity factor necessary to cause adhesion failure. The results of this modified pull test were very promising and indicated that additional investigation to determine the optimum gold release layer parameters could increase the crack propagation and lead to even more precise measurements. The ease of analysis, as compared to the scratch test, makes this an attractive procedure.

Effects of Ion Beam Mixing

Scratch testing indicated a significant adhesion improvement as the result of ion beam mixing for chromium films on sapphire substrates. The analysis methods showed an increase in the critical normal force

greater than 1800 percent, an increase in the critical plastic shear stress greater than 350 percent, and an increase in the critical elastic shear stress greater than 300 percent.

No increase in the adhesion of nickel films to sapphire substrates was detected using the scratch test because the film was subject to ductile extrusion, rather than de-adhesion at the interface, under the stylus.

For zirconium/sapphire specimens, critical normal load and plastic shear stress calculations made from scratch test data showed ion beam mixing improved the film adhesion by several hundred percent. The elastic analysis failed to reveal a critical stress since these films did not usually fail in compression ahead of the stylus, as assumed by the theory.

Tensile adhesion tests of the zirconium/sapphire systems utilizing a gold release layer indicated significant adhesion enhancement by ion beam mixing since both the mixed and unmixed regions had similar flaws but the mixed region withstood a greater stress (40 percent) and a greater stress intensity factor (30 percent) with no zirconium removal.

Tests exhibiting good pin/epoxy/film adhesion indicated that ion beam mixing increased the tensile adhesion of the aluminum and zirconium films to silicon nitride and silicon carbide substrates. This is supported by micrographs depicting the film response to thermal stresses, where the unmixed films de-adhere from the substrates as a result of the stresses while the mixed films have adequate adhesion to remain fixed to

the substrates. Lack of sufficient pin/epoxy/film strength necessitated the pull strength data be reported as "in excess of" the maximum value obtained in the pull test.

LIST OF REFERENCES

LIST OF REFERENCES

1. Ahn, J., Mittal, K. L., and MacQueen, R. H., "Hardness and Adhesion of Filmed Structures as Determined by the Scratch Technique," p. 134 in Adhesion Measurement of Thin Films, Thick Films, and Bulk Coatings, K. L. Mittal, ed., ASTM, Philadelphia, PA, 1978.

2. Benjamin, P., and Weaver, C., "Measurement of Adhesion of Thin Films," Proc. Royal Soc. of London A254 (1960) 163.

3. Butler, D. W., Stoddart, C.T.H., and Stuart, P. R., "The Stylus or Scratch Method for Thin Film Adhesion Measurement: Some Observations and Comments," J. Phys. D: Appl. Phys. 3(6) (1970) 877.

4. Campbell, David S., "Mechanical Properties of Thin Films," Chap. 12, p. 8 in Handbook of Thin Film Technology, Leon I. Maissel and Reinhart Glang, eds., McGraw-Hill Book Company, New York, 1970.

5. Weaver, Charles, "Adhesion of Thin Films," J. Vac. Sci. Technol. 12(1) (1975) 18.

6. Laeng, P., and Steinmann, P. A., "Adhesion Testing of Hard CVD Coatings Using the Scratch Test," p. 723 in Proc. 8th Intern. Conf. on Chemical Vapor Deposition, John M. Blocher, Jr., Guy E. Vuillard, and Georg Wahl, eds., The Electrochemical Society, Inc., Pennington, NJ, 1981.

7. Laugier, M., "The Development of the Scratch Test Technique for the Determination of the Adhesion of Coatings," Thin Solid Films 76 (1981) 289.

8. Perry, A. J., "The Adhesion of Chemically Vapour-Deposited Hard Coatings to Steel--The Scratch Test," Thin Solid Films 78 (1981) 77.

9. Perry, A. J., Laeng, P., and Hintermann, H. E., "Adhesion Measurements on Hard Thin Well-Adhering Coatings--A Review," p. 475 in Proc. 8th Intern. Conf. on Chemical Vapor Deposition, John M. Blocher, Jr., Guy E. Vuillard, and Georg Wahl, eds., The Electrochemical Society, Inc., Pennington, NJ, 1981.

10. Hammer, Barbara, Perry, A. J., Laeng, P., and Steinmann, P. A., "The Scratch Test Adhesion of TiC Deposited Industrially by Chemical Vapour Deposition on Steel," Thin Solid Films 96 (1982) 45.

11. Je, J. H., Gyarmati, E., and Naoumidis, A., "Scratch Adhesion Test of Reactively Sputtered TiN Coatings on a Soft Substrate," Thin Solid Films 136 (1986) 57.

12. Valli, J., Makela, U., and Matthews, A., "Assessment of Coating Adhesion," Surface Eng. 2(1) (1986) 49.

13. Perry, A. J., "Scratch Adhesion Testing of Hard Coatings," Thin Solid Films 107 (1983) 167.

14. Goldstein, I. S., and DeLong, R., "Evaluation of Microhardness and Scratch Testing for Optical Coatings," J. Vac. Sci. Technol. 20(3) (1982) 327.

15. Laugier, M., "Adhesion and Internal Stress in Thin Films of Aluminium," Thin Solid Films 79 (1981) 15.

16. Jacobson, S., Jonsson, B., and Sundqvist, B., "The Use of Fast Heavy Ions to Improve Thin Film Adhesion," Thin Solid Films 107 (1983) 89.

17. Weaver, C., and Parkinson, D. T., "Diffusion in Gold--Aluminium," Philos. Mag. 22, 8th Series (1970) 377.

18. Mehrotra, P. K., and Quinto, D. T., "Techniques for Evaluating Mechanical Properties of Hard Coatings," J. Vac. Sci. Technol., A3(6) (1985) 2401.

19. Kikuchi, Akira, Baba, Shigeru, and Kinbara, Akira, "Measurement of the Adhesion of Silver Films to Glass Substrates," Thin Solid Films 124 (1985) 343.

20. Chopra, Kasturi L., Thin Film Phenomena, McGraw-Hill Book Company, New York, 1969, p. 313.

21. Hamilton, G. M., and Goodman, L. E., "The Stress Field Created by a Circular Sliding Contact," J. Appl. Mech. 88 (1966) 371.

22. Perry, A. J., "The Adhesion of TiN on Steel," p. 737 in Proc. 8th Intern. Conf. on Chemical Vapor Deposition, John M. Blocher, Jr., Guy E. Vuillard, and Georg Wahl, eds., The Electrochemical Society, Inc., Pennington, NJ, 1981.

23. Perry, A. J., and Pulker, H. K., "Hardness, Adhesion, and Abrasion Resistance of TiO_2 Films on Glass," Thin Solid Films 124 (1985) 323.

24. Hamersky, Jaroslav, "Feststellung Optimaler Parameter Bei Adhasionsmessungen Unter Anwendung der Ritzmethode," Thin Solid Films 3 (1969) 263.

25. Timoshenko, S. P., and Goodier, J. N., Theory of Elasticity, 3rd Edition, McGraw-Hill Book Company, New York, 1970, pp. 409-414.

26. Takadoum, J., Pivin, J. C., Chaumont, J., and Roque-Carmes, C., "Friction and Wear of Amorphous Ni-B, Ni-P Films Obtained by Ion Implantation into Nickel," J. Mater. Sci. 20 (1985) 1480.

27. Laugier, M. T., "An Energy Approach to the Adhesion of Coatings Using the Scratch Test," Thin Solid Films 117 (1984) 243.

28. Hintermann, H. E., "Thin Solid Films to Combat Friction, Wear, and Corrosion," J. Vac. Sci. Technol. B2(4) (1984) 816.

29. Lhermitte-Sebire, I., Colmet, R., Naslain, R., Desmaison, J., Gladel, G., "The Adhesion Between Physically Vapour-Deposited or Chemically Vapour Deposited Alumina and TiC-Coated Cemented Carbides as Characterized by Auger Electron Spectroscopy and Scratch Testing," Thin Solid Films 138 (1986) 221.

30. Swindlehurst, W., "Acoustic Emission--1: Introduction," Non-Destructive Testing, June (1973) 152.

31. Pollock, A. A., "Acoustic Emission--2: Acoustic Emission Amplitudes," Non-Destructive Testing, October (1973) 264.

32. Curtis, G. J., "Acoustic Emission Energy Relates to Bond Strength," Non-Destructive Testing, October (1975) 249.

33. Perkins, R. A., and Meier, G. H., "Acoustic Emission Studies of High Temperature Oxidation," p. 176 in Proc. Symposium on High Temperature Materials Chemistry--II, Zuhair A. Munir and Daniel Cubicciotti, eds., The Electrochemical Society, Inc., Pennington, NJ, 1983.

34. Wilshaw, T. R., and Rothwell, R., "Instrumented Scratch for Measuring the Fracture Behavior of Strong Solids," Nature: Phys. Sci. 229 (1971) 155.

35. Rooum, J., and Rawlings, R. D., "Failure Mechanisms and Acoustic Emission Amplitude Distributions in Automotive Finishes," J. Mater. Sci. 17 (1982) 1745.

36. Bunnell, L. R., Crowe, J. C., and Hart, P. E., "Acoustic Emission Monitoring of Surface-Damaged Ceramic Materials," p. 341 in The Science of Ceramic Machining and Surface Finishing, National Bureau of Standards Special Publication 348, Washington, D.C., 1972.

37. Chapman, B. N., "Thin Film Adhesion," J. Vac. Sci. Technol. 11 (1974) 106.

38. Jacobsson, Roland, "Measurement of the Adhesion of Thin Films," Thin Solid Films 34 (1976) 191.

39. Collins, L. E., Perkins, J. G., and Stroud, P. T., "Effect of Ion Bombardment on the Adhesion of Aluminium Films on Glass," Thin Solid Films 4 (1969) 41.

40. Noda, Shoji, Doi, Haruo, Yamamoto, Nobuyuki, Hioki, Tatsumi, Kawamoto, Jun'ichi, and Kamigaito, Osami, "Improvement for Adhesion of Thin Metal Films on Ceramics by Ion Bombardment and the Application to Metal-Ceramic Joining," J. Mater. Sci. Letters 5 (1986) 381.

41. Auner, G., Hsieh, Y. F., Padmanabhan, K. R., Chevallier, J., and Sorensen, G., "Effect of Ion Implantation on Thin Hard Coatings," Thin Solid Films 107 (1983) 191.

42. Varchenya, S. A., and Upit, G. P., "Adhesive Strength of the Interface Between a Metal Film and Crystalline Quartz," Thin Solid Films 122 (1984) 59.

43. Jacobsson, R., and Kruse, B., "Measurement of Adhesion of Thin Evaporated Films on Glass Substrates by Means of the Direct Pull Method," Thin Solid Films 15 (1973) 71.

44. Cannon, R. M., Fisher, R. M., and Evans, A. G., "Decohesion of Thin Films from Ceramic Substrates," p. 799 in Thin Films--Interfaces and Phenomena, R. J. Nemanich, P. S. Ho, and S. S. Lau, eds., Materials Research Society, Pittsburgh, PA, 1985.

45. Picraux, S. Thomas, and Peercy, Paul S., "Ion Implantation of Surfaces," Scient. Am. 252(3) (1985) 102.

46. Basta, Nicholas, "Ion-Beam Implantation," High Technol. February (1985) 57.

47. Baglin, J.E.E., "Adhesion at Metal-Ceramic Interfaces: Ion Beam Enhancement and the Role of Contaminants," p. 3 in Thin Films: The Relationship of Structure to Properties, Carolyn Rubin Aita and K. S. SreeHarsha, eds., Materials Research Society, Pittsburgh, PA, 1985.

48. Hondros, E. D., "Bonding of Metal/Ceramic Interfaces," p. 121 in Science of Hard Materials, E. A. Almond, C. A. Brookes, and R. Warren, eds., Adam Hilger Ltd., Bristol, England, 1986.

49. Griffith, J. E., Qui, Yuanxum, and Tombrello, T. A., "Ion-Beam-Enhanced Adhesion in the Electronic Stopping Region," Nucl. Instrum. Methods 198 (1982) 607.

50. Appleton, B. R., Naramoto, H., White, C. W., Holland, O. W., McHargue, C. J., Farlow, G., Narayan, J., and Williams, J. M., "Ion Implantation, Ion Beam Mixing, and Annealing Studies of Metals in Al_2O_3, SiC, and Si_3N_4," Nucl. Instrum. Methods Phys. Res. B1 (1984) 167.

51. Tombrello, T. A., "Ion Beam Enhanced Adhesion," p. 173 in Thin Films--Interfaces and Phenomena, R. J. Nemanich, P. S. Ho, and S. S. Lau, eds., Materials Research Society, Pittsburg, PA, 1984.

52. Sood, D. K., Skinner, W. M., and Williams, J. S., "Helium and Electron Beam Induced Enhancement in Adhesion of Al, Au, and Pt Films on Glass," Nucl. Instrum. Methods Phys. Res. B7/8 (1985) 893.

53. Baglin, J.E.E., and Clark, G. J., "Ion Beam Bonding of Thin Films," Nucl. Instrum. Methods Phys. Res. B7/8 (1985) 881.

54. Lewis, M. B., and McHargue, C. J., "Ion Beam Mixing of Ceramic Alloys--Preparation and Mechanical Properties," p. 85 in Metastable Materials Formation by Ion Implantation, S. T. Picraux and W. J. Choyke, eds., Elsevier Science Publishing Company, Inc., New York, 1982.

55. Burnett, P. J., and Page, T. F., "Changing the Surface Mechanical Properties of Silicon and Alpha-Al_2O_3 by Ion Implantation," J. Mater. Sci. 19 (1984) 3524.

56. McHargue, C. J., and Yust, C. S., "Lattice Modification in Ion-Implanted Ceramics," J. Am. Ceram. Soc. 67(2) (1984) 117.

57. Hartley, N.E.W., "Mechanical Property Improvements on Ion Implanted Diamond," p. 295 in Metastable Materials Formation by Ion Implantation, S. T. Picraux and W. J. Choyke, eds., Elsevier Science Publishing Company, Inc., New York, 1982.

58. Davisson, C. M., and Manning, I., New Version of the Energy-Deposition Code E-DEP-1: Better Stopping Powers, NRL Report 8859, Naval Research Laboratory, Washington, DC, October 6, 1986.

59. Noda, S., Doi, H., Hioki, T., and Kamigaito, O., "Deformation and Cracking of Metal-Deposited Single Crystal Alumina and the Effects of Ion-Irradiation," J. Mater. Sci. Letters 4 (1985) 523.

60. Brown, William F., Jr., and Srawley, John E., Plane Strain Crack Toughness Testing of High Strength Metallic Materials, ASTM Special Technical Publication No. 410, American Society for Testing Materials, Philadelphia, PA, 1967, p. 12.

61. Ion Implant Profile Code, Surface Alloys Corporation, Danvers, MA, 1987.

62. Encyclopedia of Engineering Materials and Processes, H. R. Clauser, ed. in chief, Reinhold Publishing Corporation, New York, 1963, p. 149.

63. Encyclopedia of Engineering Materials and Processes, H. R. Clauser, ed. in chief, Reinhold Publishing Corporation, New York, 1963, p. 768.

64. Encyclopedia of Engineering Materials and Processes, H. R. Clauser, ed. in chief, Reinhold Publishing Corporation, New York, 1963, p. 440.

65. Ross, Robert B., Metallic Materials Specification Handbook, Third Edition, E. & F. N. Spon, London, 1980, p. 4.

VITA

Janet E. Pawel was born on December 24, 1962, in Oak Ridge, Tennessee. After graduating from Oak Ridge High School in June 1981, she entered The University of Tennessee, Knoxville and received a B.S. degree in Engineering Science and Mechanics in June 1985. Study toward an M.S. degree in Engineering Science and Mechanics at The University of Tennessee began in the Summer of 1985 and this degree was awarded in June 1987. She plans to continue her education by entering the Ph.D. program in Materials Engineering at Vanderbilt University in the Fall of 1987. Career goals include basic materials research and teaching.

The author is a student member of the American Society for Metals, the National Society of Professional Engineers (EIT), and Tau Beta Pi National Engineering Honor Society.